

1 **A comprehensive study of hygroscopic properties of calcium- and magnesium-**
2 **containing salts: implication for hygroscopicity of mineral dust and sea salt aerosols**

3
4 Liya Guo,^{1,5,a} Wenjun Gu,^{1,5,a} Chao Peng,^{2,5} Weigang Wang,² Yong Jie Li,³ Taomou Zong,⁴ Yujing
5 Tang,¹ Zhijun Wu,⁴ Qin hao Lin,¹ Maofa Ge,^{2,5,6} Guohua Zhang,¹ Min Hu,⁴ Xinhui Bi,¹ Xinming
6 Wang,^{1,5,6} Mingjin Tang^{1,5,6,*}

7
8 1 State Key Laboratory of Organic Geochemistry and Guangdong Key Laboratory of
9 Environmental Protection and Resources Utilization, Guangzhou Institute of Geochemistry,
10 Chinese Academy of Sciences, Guangzhou 510640, China

11 2 State Key Laboratory for Structural Chemistry of Unstable and Stable Species, Institute of
12 Chemistry, Chinese Academy of Sciences, Beijing 100190, China

13 3 Department of Civil and Environmental Engineering, Faculty of Science and Technology,
14 University of Macau, Avenida da Universidade, Taipa, Macau, China

15 4 State Key Joint Laboratory of Environmental Simulation and Pollution Control, College of
16 Environmental Sciences and Engineering, Peking University, Beijing 100871, China

17 5 University of Chinese Academy of Sciences, Beijing 100049, China

18 6 Center for Excellence in Regional Atmospheric Environment, Institute of Urban Environment,
19 Chinese Academy of Sciences, Xiamen 361021, China

20
21 ^a These two authors contributed equivalently to this work.

22 * Correspondence: Mingjin Tang (mingjintang@gig.ac.cn)

23 **Abstract**

24 Calcium- and magnesium-containing salts are important components for mineral dust and
25 sea salt aerosols, but their physicochemical properties are not well understood yet. In this study,
26 hygroscopic properties of eight Ca- and Mg-containing salts, including $\text{Ca}(\text{NO}_3)_2 \cdot 4\text{H}_2\text{O}$,
27 $\text{Mg}(\text{NO}_3)_2 \cdot 6\text{H}_2\text{O}$, $\text{MgCl}_2 \cdot 6\text{H}_2\text{O}$, $\text{CaCl}_2 \cdot 6\text{H}_2\text{O}$, $\text{Ca}(\text{HCOO})_2$, $\text{Mg}(\text{HCOO})_2 \cdot 2\text{H}_2\text{O}$,
28 $\text{Ca}(\text{CH}_3\text{COO})_2 \cdot \text{H}_2\text{O}$ and $\text{Mg}(\text{CH}_3\text{COO})_2 \cdot 4\text{H}_2\text{O}$, were investigated using two complementary
29 techniques. A vapor sorption analyzer was used to measure the change of sample mass with relative
30 humidity (RH) under isotherm conditions, and the deliquescence relative humidities (DRH) for
31 temperature in the range of 5-30 °C as well as water-to-solute ratios as a function of RH at 5 and
32 25 °C were reported for these eight compounds. DRH values showed large variation for these
33 compounds; for example, at 25 °C DRH were measured to be ~28.5% for $\text{CaCl}_2 \cdot 6\text{H}_2\text{O}$ and >95%
34 for $\text{Ca}(\text{HCOO})_2$ and $\text{Mg}(\text{HCOO})_2 \cdot 2\text{H}_2\text{O}$. We further found that the dependence of DRH on
35 temperature can be approximated by the Clausius-Clapeyron equation. In addition, a humidity-
36 tandem differential mobility analyzer was used to measure the change in mobility diameter with
37 RH (up to 90%) at room temperature, in order to determine hygroscopic growth factors of aerosol
38 particles generated by atomizing water solutions of these eight compounds. All the aerosol
39 particles studied in this work, very likely to be amorphous under dry conditions, started to grow at
40 very low RH (as low as 10%) and showed continuous growth with RH. Hygroscopic growth factors
41 at 90% RH were found to range from 1.26 ± 0.04 for $\text{Ca}(\text{HCOO})_2$ to 1.79 ± 0.03 for $\text{Ca}(\text{NO}_3)_2$, and
42 the single hygroscopicity parameter ranged from 0.09-0.13 for $\text{Ca}(\text{CH}_3\text{COO})_2$ to 0.49-0.56 for
43 $\text{Ca}(\text{NO}_3)_2$. Overall, our work provides a comprehensive investigation of hygroscopic properties of
44 these Ca- and Mg-containing salts, largely improving our knowledge in the physicochemical
45 properties of mineral dust and sea salt aerosols.

46 **1 Introduction**

47 Mineral dust, mainly emitted from arid and semi-arid regions with an annual flux of
48 ~2000 Tg, is one of the most abundant types of aerosols in the troposphere (Textor et al., 2006;
49 Ginoux et al., 2012). Mineral dust aerosol affects the climate system directly by scattering and
50 absorbing solar and terrestrial radiation (Formenti et al., 2011; Ridley et al., 2016; Chen et al.,
51 2017) and indirectly by serving as cloud condensation nuclei (CCN) and ice nucleating particles
52 (INPs) (Hoose and Moehler, 2012; Creamean et al., 2013; Cziczo et al., 2013; Tang et al., 2016a).
53 In addition, deposition of mineral dust particles is an important source of several nutrient elements
54 (Fe and P, for example) for many ecosystems around the globe, thus having significant impacts on
55 biogeochemical cycles in these regions (Jickells et al., 2005; Mahowald et al., 2009; Mahowald et
56 al., 2011; Zhang et al., 2015).

57 Mineral dust aerosol has an average lifetime of 2-7 days in the atmosphere and can thus be
58 transported over thousands of kilometers (Textor et al., 2006; Uno et al., 2009). During transport
59 mineral dust particles may undergo heterogeneous reactions with trace gases, impacting the
60 abundance of a number of important reactive trace gases both directly and indirectly (Usher et al.,
61 2003; Crowley et al., 2010; Romanias et al., 2012; Tang et al., 2017). These reactions can also lead
62 to change in chemical composition of mineral dust particles (Usher et al., 2003; Li and Shao, 2009;
63 Li et al., 2010; Tang et al., 2012; Romanias et al., 2016) and thereby modification of their
64 physicochemical and optical properties (Krueger et al., 2003; Vlasenko et al., 2006; Liu et al.,
65 2008b; Sullivan et al., 2009; Tang et al., 2016a; Pan et al., 2017). Mineral dust particles contain
66 substantial amounts of carbonates, including CaCO_3 (calcite) and $\text{CaMg}(\text{CO}_3)_2$ (dolomite)
67 (Nickovic et al., 2012; Formenti et al., 2014; Jeong and Achterberg, 2014; Journet et al., 2014;
68 Scanza et al., 2015). These carbonates are largely insoluble and have very low hygroscopicity

69 (Sullivan et al., 2009; Tang et al., 2016a); however, their reactions with acidic gases in the
70 troposphere can form Ca- and Mg-containing salts with higher hygroscopicity (Gibson et al., 2006;
71 Liu et al., 2008b; Sullivan et al., 2009; Tang et al., 2016a), such as $\text{Ca}(\text{NO}_3)_2$ and $\text{Mg}(\text{NO}_3)_2$. For
72 example, numerous laboratory and field studies have found that due to the formation of $\text{Ca}(\text{NO}_3)_2$
73 and CaCl_2 from heterogeneous reactions with nitrogen oxides (Goodman et al., 2000; Liu et al.,
74 2008a; Li et al., 2010; Tang et al., 2012; Tan et al., 2016) and HCl (Santschi and Rossi, 2006),
75 solid CaCO_3 particles could be converted to aqueous droplets under tropospheric conditions
76 (Krueger et al., 2003; Laskin et al., 2005; Liu et al., 2008b; Shi et al., 2008; Tobo et al., 2010). In
77 addition, MgCl_2 and CaCl_2 are important components in sea salt aerosol (as known as sea spray
78 aerosol). The presence of MgCl_2 and CaCl_2 , in addition to NaCl, can alter the hygroscopicity of
79 sea salt aerosol (Gupta et al., 2015; Zieger et al., 2017); to be more specific, the hygroscopicity of
80 sea salt was found to be significantly smaller than pure NaCl. Furthermore, the CCN activity of
81 saline mineral dust was explored (Gaston et al., 2017), and good correlations were found between
82 the CCN activities of saline mineral dust particles and the abundance of the soluble components
83 (e.g., CaCl_2) they contained.

84 Nevertheless, hygroscopic properties of $\text{Ca}(\text{NO}_3)_2$, $\text{Mg}(\text{NO}_3)_2$, CaCl_2 and MgCl_2 have not
85 been completely understood, especially in the two following aspects. First, hygroscopic growth
86 factors were only measured by one or two previous studies for $\text{Ca}(\text{NO}_3)_2$ (Gibson et al., 2006; Jing
87 et al., 2018), $\text{Mg}(\text{NO}_3)_2$ (Gibson et al., 2006), CaCl_2 (Park et al., 2009) and MgCl_2 aerosols (Park
88 et al., 2009). Considering the importance of these compounds in the troposphere, additional
89 measurements of their hygroscopic growth are clearly warranted. In addition, tropospheric
90 temperatures range from ~200 to ~300 K; however, the effects of temperature on their phase

91 transitions and hygroscopic growth remain largely unclear (Kelly and Wexler, 2005), due to lack
92 of experimental data below room temperature.

93 Small carboxylic acids, such as formic and acetic acids, are abundant in the troposphere
94 (Khare et al., 1999), and previous studies suggested that heterogeneous reactions of mineral dust
95 with formic and acetic acids are efficient (Hatch et al., 2007; Prince et al., 2008; Tong et al., 2010;
96 Ma et al., 2012; Tang et al., 2016b). It was shown that calcium and magnesium acetates were
97 formed in heterogeneous reactions of gaseous acetic acid with MgO and CaCO₃ particles, leading
98 to significant increase in particle hygroscopicity (Ma et al., 2012). However, only a few previous
99 studies explored hygroscopic growth of Mg(CH₃COO)₂ and Ca(CH₃COO)₂, using techniques
100 based on bulk samples (Wang et al., 2005; Ma et al., 2012; Pang et al., 2015). To our knowledge,
101 hygroscopic growth factors have never been reported for Ca(HCOO)₂, Mg(HCOO)₂,
102 Ca(CH₃COO)₂ and Mg(CH₃COO)₂ aerosol particles.

103 To better understand hygroscopic properties of these Ca- and Mg-containing salts, two
104 complementary techniques were employed in this work to investigate their phase transitions and
105 hygroscopic growth. A vapor sorption analyzer, which measured the sample mass as a function of
106 RH, was used to determine the DRH and solute-to-water ratios for Ca(NO₃)₂·4H₂O,
107 Mg(NO₃)₂·6H₂O, CaCl₂·6H₂O, MgCl₂·6H₂O, Ca(HCOO)₂, Mg(HCOO)₂·2H₂O,
108 Ca(CH₃COO)₂·H₂O and Mg(CH₃COO)₂·4H₂O at different temperatures (5-30 °C). Furthermore,
109 hygroscopic growth factors of Ca(NO₃)₂, Mg(NO₃)₂, CaCl₂, MgCl₂, Ca(HCOO)₂, Mg(HCOO)₂,
110 Ca(CH₃COO)₂ and Mg(CH₃COO)₂ aerosol particles were determined at room temperature up to
111 90% RH, using a humidity-tandem differential mobility analyzer. This work would significantly
112 increase our knowledge in the hygroscopicity of these compounds, hence leading to a better
113 understanding of the physicochemical properties of mineral dust and sea salt aerosols.

114 **2 Experimental section**

115 Hygroscopic growth of Ca- and Mg-containing salts were investigated using two
116 complementary techniques, i.e. a humidity-tandem differential mobility analyzer (H-TDMA) and
117 a vapor sorption analyzer (VSA). Eight salts, all supplied by Aldrich, were investigated in this
118 work, including $\text{Ca}(\text{NO}_3)_2 \cdot 4\text{H}_2\text{O}$ (>99%), $\text{Mg}(\text{NO}_3)_2 \cdot 6\text{H}_2\text{O}$ (99%), $\text{CaCl}_2 \cdot 6\text{H}_2\text{O}$ (>99%),
119 $\text{MgCl}_2 \cdot 6\text{H}_2\text{O}$ (>99%), $\text{Ca}(\text{HCOO})_2$ (>99%), $\text{Mg}(\text{HCOO})_2 \cdot 2\text{H}_2\text{O}$ (98%), $\text{Ca}(\text{CH}_3\text{COO})_2 \cdot \text{H}_2\text{O}$
120 (>99%) and $\text{Mg}(\text{CH}_3\text{COO})_2 \cdot 4\text{H}_2\text{O}$ (99%).

121 **2.1 H-TDMA experiments**

122 H-TDMA measurements were carried out at Institute of Chemistry, Chinese Academy of
123 Sciences, and the experimental setup was detailed in previous work (Lei et al., 2014; Peng et al.,
124 2016). Hygroscopic growth of size-selected aerosol particles was determined by measuring their
125 mobility diameters at different RH. An atomizer (MSP 1500) was used to generate aerosol particles.
126 Solutions used for atomization were prepared using ultrapure water, and their typical
127 concentrations were 0.3-0.4 g L⁻¹. After exiting the atomizer, an aerosol flow (300 mL/min) was
128 passed through a Nafion dryer and then a diffusion dryer filled with silica gel to reach a final RH
129 of <5%. The aerosol flow was then delivered through a neutralizer and the first differential
130 mobility analyzer (DMA) to produce quasi-monodisperse aerosol particles with a mobility
131 diameter of 100 nm. After that, the aerosol flow was transferred through a humidification section
132 with a residence time of ~27 s to be humidified to a given RH. The humidification section was
133 made of two Nafion humidifiers (MD-700-12F-1, Perma Pure) connected in series. The RH of the
134 resulting aerosol flow was monitored using a dew-point meter, which had an absolute uncertainty
135 of ±0.8% in RH measurement as stated by the manufacturer (Michell, UK). After humidification,
136 the size distribution of aerosol particles was measured using a scanning mobility particle sizer

137 (SMPS) which consisted of the second DMA coupled with a condensation particle counter (TSI
138 3776). For the second DMA, the aerosol flow and the sheath flow were always maintained at the
139 same RH. The flow rate ratios of the aerosol flow to the sheath flow were set to 1:10 for both
140 DMA.

141 In our work, the hygroscopic growth factor (GF) is defined as the ratio of measured
142 mobility diameters at a given RH to that at dry conditions:

$$143 \quad GF = \frac{d}{d_0} \quad (1)$$

144 where d_0 and d are the measured mobility diameters at <5% RH and at a given RH, respectively.
145 In our work the dry mobility diameter selected using the first DMA was always 100 nm, and no
146 shape factors were used to correct the dry particle diameters. Size distributions of all the eight
147 types of aerosol particles, measured using the SMPS, were found to be unimode, as illustrated by
148 Figure S1 (in the supplementary information) in which size distributions of $\text{Ca}(\text{NO}_3)_2$ aerosols at
149 4, 50 and 90% RH are displayed as an example. The TDMAinv algorithm (Gysel et al., 2009) was
150 applied to the H-TDMA data.

151 All the experiments were carried out at room temperature (298 ± 1 K), and in each
152 experiment hygroscopic growth of aerosol particles was determined at 12 different RH, i.e. <5, 10,
153 20, 30, 40, 50, 60, 70, 75, 80, 85, and 90%. The absolute uncertainties in RH were estimated to be
154 within $\pm 2\%$. Hygroscopic growth of each compound was measured three times. The performance
155 of the H-TDMA setup was routinely checked by measuring the hygroscopic growth of 100 nm
156 $(\text{NH}_4)_2\text{SO}_4$ and NaCl aerosol particles. Good agreement between measured hygroscopic growth
157 curves with those predicted using the E-AIM model (Clegg et al., 1998) was always found for
158 $(\text{NH}_4)_2\text{SO}_4$ and NaCl aerosols, as detailed in our previous work (Jing et al., 2016; Peng et al., 2016).

159 2.2 VSA experiments

160 The vapor sorption analyzer (Q5000SA), which measured the mass of a bulk sample as a
161 function of RH under isotherm conditions, was manufactured by TA Instruments (New Castle, DE,
162 USA). These experiments were performed at Guangzhou Institute of Geochemistry, Chinese
163 Academy of Sciences, and the instrument and experimental method were described elsewhere (Gu
164 et al., 2017a; Gu et al., 2017b; Jia et al., 2018). Experiments could be conducted in a temperature
165 range of 5-85 °C with an accuracy of ± 0.1 °C and a RH range of 0-98% with an absolute accuracy
166 of $\pm 1\%$. The mass measurement had a range of 0-100 mg, and its sensitivity was stated to be < 0.1
167 μg . Initial mass of samples used in an experiment was usually in the range of 0.5-1 mg.

168 Two different types of experiments were carried out. The mass hygroscopic growth was
169 studied in the first type of experiments: after the sample was dried at $< 1\%$ RH as a given
170 temperature, RH was increased to 90% stepwise with an increment of 10% per step; after that, RH
171 was set to 0% (the actual RH was measured to be $< 1\%$) to dry the sample again. The second type
172 of experiments were conducted to measure DRH values: the sample was first dried at a given
173 temperature, and RH was increased to a value which was at least 5% lower than the expected DRH;
174 RH was then increased stepwise with an increment of 1% until a significant increase in sample
175 mass was observed, and the RH at which the sample mass showed a significant increase was equal
176 to its DRH. The measured relative change in sample mass due to signal noise and baseline drift
177 was $< 0.5\%$ in our work; in each experiment when we suspected that the sample were undergoing
178 deliquescence at a certain RH, we did not stop the experiment until the mass increase was $> 5\%$ to
179 ensure the occurrence of deliquescence. At each RH the sample was considered to reach
180 equilibrium with the environment when its mass change was $< 0.1\%$ within 30 min, and RH was
181 changed to the next value only after the sample mass was stabilized. If the sample mass was

182 increasing steadily but with a very small rate (e.g., <0.1% in 30 min), the program we used may
183 conclude erroneously that the system had reached the equilibrium; therefore, all the experimental
184 data were inspected to check whether at each RH the sample mass reached the plateau (i.e. the
185 system had reached the equilibrium). The time to reach a new equilibrium varied with compounds
186 and largely depended on the dry sample mass, i.e. a sample with larger dry mass would took longer
187 to reach the equilibrium. Each experiment was repeated at least three times, and the average value
188 and standard deviation were reported.

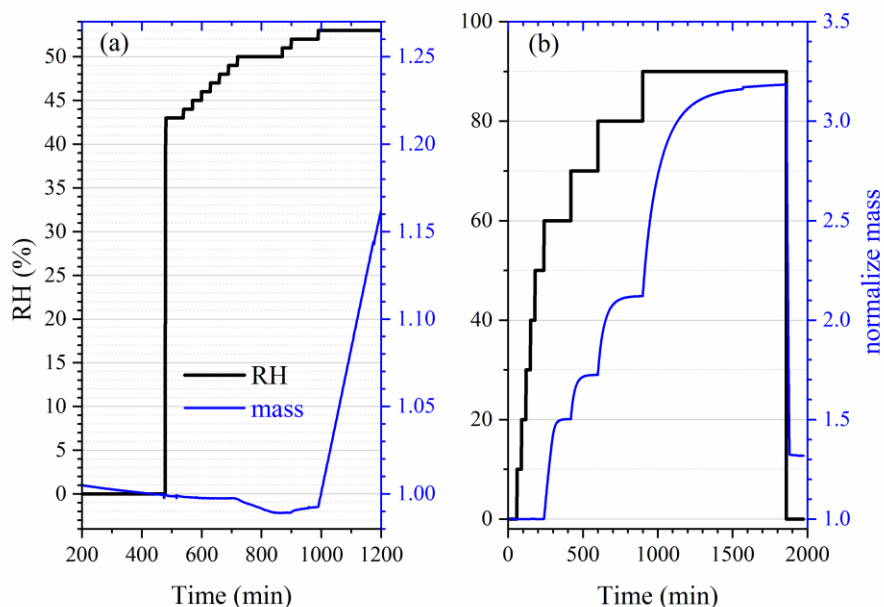
189 **3 Results and discussion**

190 **3.1 Hygroscopicity of nitrates and chlorides**

191 **3.1.1 DRH at different temperature**

192 First we investigated the effect of temperature on the DRH of $\text{Ca}(\text{NO}_3)_2 \cdot 4\text{H}_2\text{O}$,
193 $\text{Mg}(\text{NO}_3)_2 \cdot 6\text{H}_2\text{O}$ and $\text{MgCl}_2 \cdot 6\text{H}_2\text{O}$, which are the most stable forms of corresponding salts for the
194 temperature range (5-30 °C) considered in this work (Kelly and Wexler, 2005). Figure 1a shows
195 the change of RH and normalized sample mass as a function of time in an experiment to measure
196 the DRH of $\text{Mg}(\text{NO}_3)_2 \cdot 6\text{H}_2\text{O}$ at 25 °C. Abrupt and significant increase in sample mass was
197 observed when RH was increased from 52 to 53%, suggesting that the deliquescence occurred
198 between 52 and 53% RH. Therefore, its DRH was measured to be 52.5 ± 0.5 %; since RH for our
199 VSA instrument had an absolute uncertainty of $\pm 1\%$ (as stated in Section 2.2), in our work an
200 uncertainty of $\pm 1\%$, instead of $\pm 0.5\%$, was assigned to the measured DRH. It should be noted that
201 the mass change was >15% when RH was increased from 52 to 53%, as shown in Figure 1a; such
202 a large mass increase cannot be solely caused by water adsorption, since the mass of several
203 monolayers of adsorbed water is estimated to be <1% of the dry particle mass (Gu et al., 2017b).
204 The continuous but small decrease in sample mass (about 1% in total) with time (around 500-1000

205 min) before deliquescence took place, as shown in Figure 1a, was likely caused by desorption of
206 residual water contained by the sample under investigation.



207
208 **Figure 1.** Change of normalized sample mass (blue curve, right y-axis) and RH (black curve, left
209 y-axis) as a function of time. (a) A typical experiment conducted to measure the DRH; (b) A typical
210 experiment conducted to measure mass hygroscopic growth factors. In the two experiments shown
211 here, $\text{Mg}(\text{NO}_3)_2 \cdot 6\text{H}_2\text{O}$ was investigated at 25 °C. In this paper the sample mass was always
212 normalized to its dry mass.

213
214 Table 1 summarizes our measured DRH of $\text{Ca}(\text{NO}_3)_2 \cdot 4\text{H}_2\text{O}$, $\text{Mg}(\text{NO}_3)_2 \cdot 6\text{H}_2\text{O}$ and
215 $\text{MgCl}_2 \cdot 6\text{H}_2\text{O}$ as a function of temperature (5-30 °C). DRH values show a strong dependence on
216 temperature for $\text{Ca}(\text{NO}_3)_2 \cdot 4\text{H}_2\text{O}$ (decreasing from 60.5% at 5 °C to 46.0% at 30 °C) and a weaker
217 temperature dependence for $\text{Mg}(\text{NO}_3)_2 \cdot 6\text{H}_2\text{O}$ (decreasing from 57.5% at 5 °C to 50.5% at 30 °C);
218 in contrast, the DRH values of $\text{MgCl}_2 \cdot 6\text{H}_2\text{O}$ (31.5-32.5 %) exhibit little variation with temperature

219 (5-30 °C). Several previous studies have reported the DRH of $\text{Ca}(\text{NO}_3)_2 \cdot 4\text{H}_2\text{O}$, $\text{Mg}(\text{NO}_3)_2 \cdot 6\text{H}_2\text{O}$
 220 and $\text{MgCl}_2 \cdot 6\text{H}_2\text{O}$, and their results are compared with our work in the following paragraphs.

221
 222 **Table 1.** DRH (in %) of $\text{Ca}(\text{NO}_3)_2 \cdot 4\text{H}_2\text{O}$, $\text{Mg}(\text{NO}_3)_2 \cdot 6\text{H}_2\text{O}$ and $\text{MgCl}_2 \cdot 6\text{H}_2\text{O}$ measured in this work
 223 as a function of temperatures (5-30 °C). Solubility data (mol per kg water) compiled by Kelly and
 224 Wexler (2005) was used to calculate solubilities in mol per mol water. All the errors given in this
 225 work are standard deviations.

T (°C)	$\text{Ca}(\text{NO}_3)_2 \cdot 4\text{H}_2\text{O}$	$\text{Mg}(\text{NO}_3)_2 \cdot 6\text{H}_2\text{O}$	$\text{MgCl}_2 \cdot 6\text{H}_2\text{O}$
5	60.5±1.0	57.5±1.0	32.5±1.0
10	58.0±1.0	56.5±1.0	32.5±1.0
15	55.5±1.0	54.5±1.0	32.5±1.0
20	52.5±1.0	53.5±1.0	32.5±1.0
25	49.5±1.0	52.5±1.0	31.5±1.0
30	46.0±1.0	50.5±1.0	31.5±1.0
solubility (mol per kg water)	8.4	4.9	5.84
solubility (A, mol per mol water)	0.1512	0.0882	0.1051
$A \cdot \Delta H_s / R$ (K)	913±59	427±28	--
ΔH_s (kJ mol ⁻¹)	50.2±3.3	40.3±2.6	--

226 The $A \cdot \Delta H_s / R$ and ΔH_s values were not estimated for $\text{MgCl}_2 \cdot 6\text{H}_2\text{O}$ because the difference in its measured
 227 DRH between 5 and 30 °C was very small or even insignificant. Please refer to Section 3.1.1 for further
 228 details.

229
 230 **$\text{Ca}(\text{NO}_3)_2 \cdot 4\text{H}_2\text{O}$:** RH of air in equilibrium with saturated $\text{Ca}(\text{NO}_3)_2 \cdot 4\text{H}_2\text{O}$ solutions, i.e.
 231 the DRH values of $\text{Ca}(\text{NO}_3)_2 \cdot 4\text{H}_2\text{O}$, were measured to be 55.9, 55.4, 50.5 and 46.7% at 15, 20, 25
 232 and 30 °C (Adams and Merz, 1929), and the absolute differences between DRH reported by Adams
 233 and Merz (1929) and those measured in our work are <3%. The water vapor pressures of saturated
 234 $\text{Ca}(\text{NO}_3)_2 \cdot 4\text{H}_2\text{O}$ solutions were measured to be 0.693, 0.920, 1.253, 1.591 and 1.986 kPa at 10, 15,

235 20, 25 and 30 °C (Apelblat, 1992), corresponding to DRH of 56, 54, 54, 50 and 47%, respectively;
236 therefore, the absolute difference between DRH measured in our work and those derived from
237 Apelblat (1992) are <2%. In another study (Al-Abadleh et al., 2003), RH over the saturated
238 $\text{Ca}(\text{NO}_3)_2 \cdot 4\text{H}_2\text{O}$ solution was measured to be $57 \pm 5\%$ at room temperature; in other words, Al-
239 Abadleh et al. (2003) reported a DRH of $57 \pm 5\%$ for $\text{Ca}(\text{NO}_3)_2 \cdot 4\text{H}_2\text{O}$, slightly larger than that
240 ($49.5 \pm 1.0\%$ at 25 °C) determined in our work.

241 **$\text{Mg}(\text{NO}_3)_2 \cdot 6\text{H}_2\text{O}$:** Water vapor pressures of saturated $\text{Mg}(\text{NO}_3)_2 \cdot 6\text{H}_2\text{O}$ solutions were
242 determined to be 0.737, 1.017, 1.390, 1.813 and 2.306 kPa at 10, 15, 20, 25 and 30 °C (Apelblat,
243 1992), giving DRH of 60, 60, 59, 57 and 54% at corresponding temperatures. The vapor pressure
244 of saturated $\text{Mg}(\text{NO}_3)_2 \cdot 6\text{H}_2\text{O}$ solutions at 25 °C were reported to be 1.674 and 1.666 kPa by another
245 two studies (Biggs et al., 1955; Robinson and Stokes, 1959), corresponding to DRH of ~53%. In
246 addition, the water activity of the saturated $\text{Mg}(\text{NO}_3)_2$ solution was measured to be 0.528 at 25 °C
247 (Rard et al., 2004), also suggesting a DRH value of ~53%; similarly, RH over the saturated
248 $\text{Mg}(\text{NO}_3)_2$ solution was reported to be ~53% at 22-24 °C (Li et al., 2008b). Al-Abadleh and
249 Grassian (2003) investigated the phase transition of the $\text{Mg}(\text{NO}_3)_2 \cdot 6\text{H}_2\text{O}$ film, and its DRH was
250 determined to be 49-54% at 23 °C. As shown in Table 1, DRH measured in our work agree very
251 well with those reported by most of previous studies (Biggs et al., 1955; Robinson and Stokes,
252 1959; Al-Abadleh and Grassian, 2003; Rard et al., 2004), but are always 3-5% lower than those
253 derived from Apelblat (1992). **It is not clear why DRH values measured by Apelblat (1992) at**
254 **different temperatures are always slightly higher than other studies.**

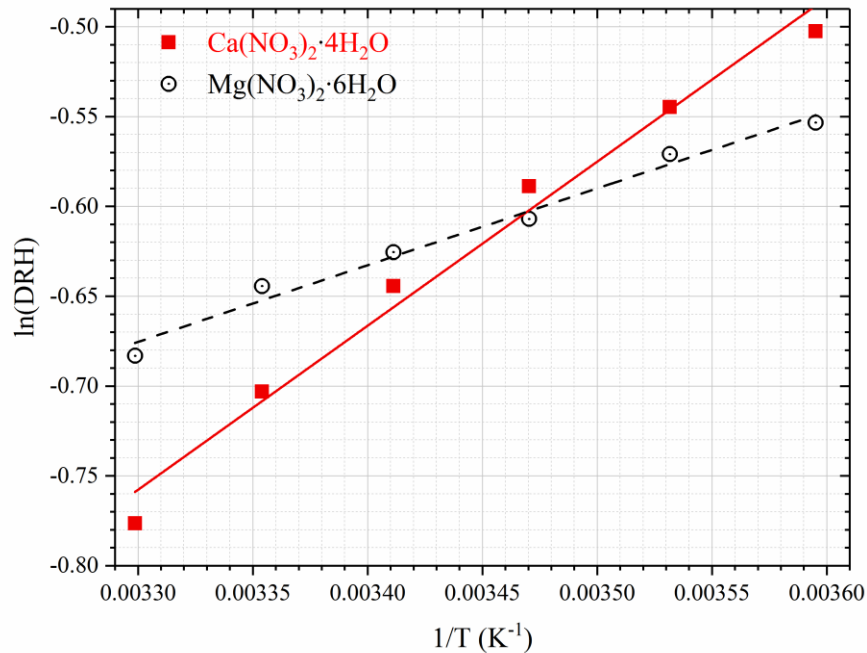
255 **$\text{MgCl}_2 \cdot 6\text{H}_2\text{O}$:** Kelly and Wexler (2005) calculated DRH of $\text{MgCl}_2 \cdot 6\text{H}_2\text{O}$ from vapor
256 pressures of saturated $\text{MgCl}_2 \cdot 6\text{H}_2\text{O}$ solutions measured by previous work, and found that DRH
257 values were in the range of 33-34% for temperatures at 0-40 °C. In addition, water activity of the

258 saturated MgCl_2 solution was reported to be 0.3278 at 25 °C (Rard and Miller, 1981),
259 corresponding to a DRH value of ~33% for $\text{MgCl}_2 \cdot 6\text{H}_2\text{O}$. The DRH values of $\text{MgCl}_2 \cdot 6\text{H}_2\text{O}$
260 measured in our work, as summarized in Table 1, show excellent agreement with those reported
261 by previous work (Rard and Miller, 1981; Kelly and Wexler, 2005). Phase transition and
262 deliquescence behavior of $\text{CaCl}_2 \cdot 6\text{H}_2\text{O}$ were also investigated in our work and found to be very
263 complex, and the result will be discussed in Section 3.1.3.

264 Temperature in the troposphere varies from ~200 to >300 K, and it is thus warranted to
265 explore the effects of temperature on hygroscopic properties of atmospherically relevant particles.
266 The dependence of DRH on temperature can usually be approximated by the Clausius-Clapeyron
267 equation (Wexler and Seinfeld, 1991; Seinfeld and Pandis, 2016; Jia et al., 2018):

$$268 \quad \ln[DRH(T)] = \ln[DRH(298)] + \frac{A \cdot \Delta H_s}{R} \left(\frac{1}{T} - \frac{1}{298} \right) \quad (2)$$

269 where T is temperature (K), $DRH(T)$ and $DRH(298)$ are the DRH at T and 298 K, R is the gas
270 constant ($8.314 \text{ J mol}^{-1} \text{ K}^{-1}$), and ΔH_s is the enthalpy of dissolution (J mol^{-1}). The dimensionless
271 constant, A , is numerically equal to the water solubility of the salt under investigation in the unit
272 of mol per mol water. Figure 2 shows the dependence of DRH values on temperature for
273 $\text{Ca}(\text{NO}_3)_2 \cdot 4\text{H}_2\text{O}$ and $\text{Mg}(\text{NO}_3)_2 \cdot 6\text{H}_2\text{O}$, confirming that Eq. (2) can indeed approximate the
274 temperature dependence. The slope, which is equal to $A \cdot \Delta H_s / R$, was determined to be $913 \pm 59 \text{ K}$
275 for $\text{Ca}(\text{NO}_3)_2 \cdot 4\text{H}_2\text{O}$ and $427 \pm 28 \text{ K}$ for $\text{Mg}(\text{NO}_3)_2 \cdot 6\text{H}_2\text{O}$, and thus ΔH_s was derived to be 50.2 ± 3.3
276 kJ mol^{-1} for $\text{Ca}(\text{NO}_3)_2 \cdot 4\text{H}_2\text{O}$ and $40.3 \pm 2.6 \text{ kJ mol}^{-1}$ for $\text{Mg}(\text{NO}_3)_2 \cdot 6\text{H}_2\text{O}$. It should be noted that
277 for Eq. (2) to be valid, both the enthalpy of dissolution and the water solubility are assumed to be
278 constant for the temperature range considered. The variation of DRH with temperature (5-30 °C)
279 was very small and even insignificant for $\text{MgCl}_2 \cdot 6\text{H}_2\text{O}$; as a result, we did not attempt to estimate
280 the ΔH_s values for $\text{MgCl}_2 \cdot 6\text{H}_2\text{O}$ since such estimation would have large errors.



281

282 **Figure 2.** Dependence of DRH on temperature for $\text{Ca}(\text{NO}_3)_2 \cdot 4\text{H}_2\text{O}$ and $\text{Mg}(\text{NO}_3)_2 \cdot 6\text{H}_2\text{O}$.

283 **3.1.2 Water-to-solute ratios as a function of RH**

284 The change of sample mass with RH (0-90%) was measured at 5 and 25 °C for
 285 $\text{Ca}(\text{NO}_3)_2 \cdot 4\text{H}_2\text{O}$, $\text{Mg}(\text{NO}_3)_2 \cdot 6\text{H}_2\text{O}$ and $\text{MgCl}_2 \cdot 6\text{H}_2\text{O}$, using the vapor sorption analyzer. The mass
 286 change, relative to that at 0% RH, can be used to calculate water-to-solute ratios (WSR, defined in
 287 this work as the molar ratio of H_2O to Ca^{2+} or Mg^{2+}) for deliquesced samples. Small increases in
 288 m/m_0 (typically <2%) were observed for some compounds (as shown in Tables 2 and 6) when RH
 289 was below corresponding DRH values, mainly due to water adsorption/desorption and baseline
 290 drift. As summarized in Table 2, decrease in temperature would lead to increase in WSR at a given
 291 RH: at 90% RH for example, WSR were determined to be 28.78 ± 0.20 at 25 °C and 31.80 ± 0.96 at
 292 5 °C for $\text{Ca}(\text{NO}_3)_2 \cdot 4\text{H}_2\text{O}$, 36.87 ± 0.23 at 25 °C and 41.40 ± 1.36 at 5 °C for $\text{Mg}(\text{NO}_3)_2 \cdot 6\text{H}_2\text{O}$, and
 293 36.26 ± 1.76 at 25 °C and 39.55 ± 2.43 at 5 °C for $\text{MgCl}_2 \cdot 6\text{H}_2\text{O}$, respectively. As discussed in Section
 294 3.1.1, the enthalpies of dissolution (ΔH_s) are negative for these compounds, suggesting that their

295 dissolution processes in water are exothermic; therefore, dissolution is favored at lower
 296 temperatures and at a given RH, decrease in temperature would lead to increase in WSR in the
 297 aqueous solutions. Several previous studies have measured RH over aqueous $\text{Ca}(\text{NO}_3)_2$, $\text{Mg}(\text{NO}_3)_2$
 298 and MgCl_2 solutions at given concentrations, and their results are compared with our work, as
 299 discussed below.

300
 301 **Table 2.** Mass growth factors (m/m_0 , defined as the ratio of sample mass at a given RH to that at
 302 0% RH) and water-to-solute ratios (WSR) as a function of RH (0-90%) at 25 and 5 °C for
 303 $\text{Ca}(\text{NO}_3)_2 \cdot 4\text{H}_2\text{O}$, $\text{Mg}(\text{NO}_3)_2 \cdot 6\text{H}_2\text{O}$ and $\text{MgCl}_2 \cdot 6\text{H}_2\text{O}$. WSR were only calculated for RH exceeding
 304 the DRH (i.e. when the sample was deliquesced). All the errors given in this work are standard
 305 deviations.

		Ca(NO ₃) ₂ ·4H ₂ O, 25 °C		Ca(NO ₃) ₂ ·4H ₂ O, 5 °C	
RH (%)	m/m_0	WSR	m/m_0	WSR	
0	1.000±0.001	--	1.000±0.001	--	
10	1.000±0.001	--	1.001±0.001	--	
20	1.014±0.005	--	1.005±0.003	--	
30	1.016±0.007	--	1.005±0.002	--	
40	1.017±0.009	--	1.009±0.003	--	
50	1.237±0.006	7.10±0.03	1.032±0.005	--	
60	1.363±0.008	8.76±0.05	1.041±0.002	--	
70	1.550±0.009	11.22±0.06	1.610±0.010	12.00±0.07	
80	1.897±0.012	15.77±0.10	1.979±0.027	16.85±0.23	
90	2.889±0.020	28.78±0.20	3.119±0.095	31.80±0.96	
		Mg(NO ₃) ₂ ·6H ₂ O, 25 °C		Mg(NO ₃) ₂ ·6H ₂ O, 5 °C	
RH (%)	m/m_0	WSR	m/m_0	WSR	
0	1.000±0.001	--	1.000±0.001	--	
10	1.000±0.001	--	1.000±0.001	--	
20	1.000±0.001	--	1.000±0.001	--	

30	1.001±0.001	--	1.000±0.001	--
40	1.001±0.001	--	1.000±0.001	--
50	1.000±0.001	--	1.000±0.001	--
60	1.503±0.001	13.15±0.01	1.539±0.003	13.67±0.03
70	1.724±0.001	16.30±0.01	1.773±0.007	16.99±0.07
80	2.121±0.001	21.94±0.01	2.203±0.021	23.11±0.22
90	3.171±0.029	36.87±0.23	3.489±0.114	41.40±1.36
MgCl ₂ ·6H ₂ O, 25 °C			MgCl ₂ ·6H ₂ O, 5 °C	
RH (%)	<i>m/m</i> ₀	WSR	<i>m/m</i> ₀	WSR
0	1.000±0.001	--	1.000±0.001	--
10	1.000±0.001	--	1.000±0.001	--
20	1.000±0.001	--	1.000±0.001	--
30	1.001±0.001	--	1.000±0.001	--
40	1.344±0.057	9.89±0.42	1.327±0.082	9.69±0.60
50	1.489±0.062	11.52±0.48	1.473±0.090	11.34±0.69
60	1.677±0.072	13.65±0.58	1.667±0.100	13.52±0.82
70	1.951±0.084	16.74±0.72	1.950±0.117	16.72±1.00
80	2.433±0.117	22.18±1.06	2.465±0.148	22.54±1.35
90	3.681±0.178	36.26±1.76	3.972±0.244	39.55±2.43

306

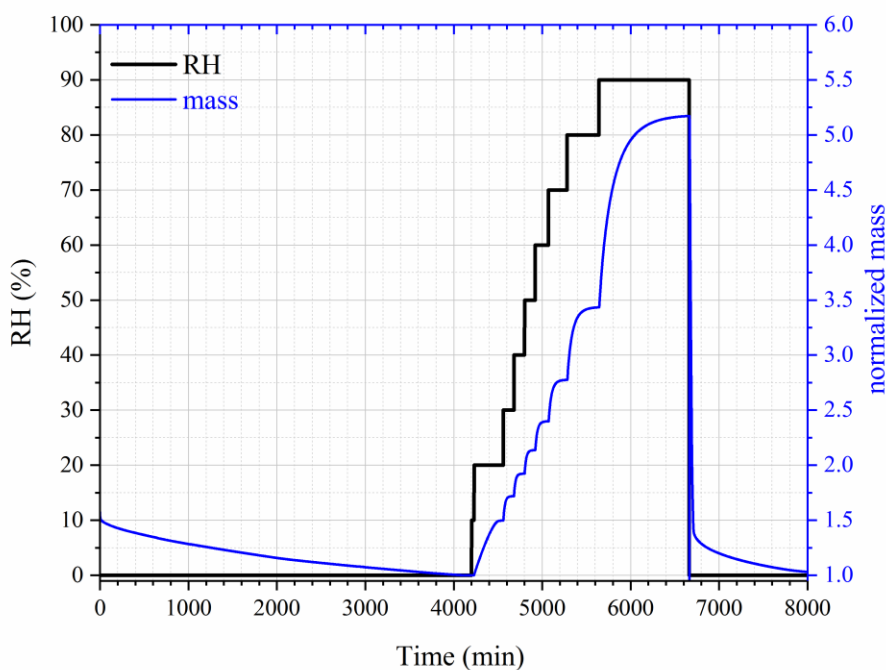
307 **Ca(NO₃)₂:** Water activities of Ca(NO₃)₂ solutions at 25 °C were measured to be 0.904,
308 0.812 and 0.712 when the concentrations were 2.0, 3.5 and 5.0 mol kg⁻¹, respectively (El
309 Guendouzi and Marouani, 2003). Since water activity of a solution is equal to the RH of air in
310 equilibrium with the solution, it can be derived that the molality concentrations of Ca(NO₃)₂
311 solution were 2.0, 3.5 and 5.0 mol kg⁻¹ when RH was 90.4, 81.2 and 71.2%; in other words, WSR
312 were found to be 11.1, 15.9 and 27.8 at 71.2, 81.2 and 90.4 % RH, respectively (El Guendouzi and
313 Marouani, 2003). As shown in Table 2, in our work WSR were determined to be 11.22±0.06,
314 15.77±0.10 and 28.78±0.20 at 70, 80 and 90% RH for Ca(NO₃)₂ solutions at the same temperature,
315 suggesting good agreement with El Guendouzi and Marouani (2003).

316 **Mg(NO₃)₂:** Water activities of Mg(NO₃)₂ solutions were reported to be 0.897, 0.812 and
317 0.702 when the concentrations of the bulk solutions were 1.6, 2.5 and 3.5 mol kg⁻¹ at 25 °C,
318 respectively (Rard et al., 2004); this means that WSR were equal to 15.9, 22.2 and 34.7 at 70.2,
319 81.2 and 89.7% RH. Ha and Chan (1999) fitted their measured water activities of Mg(NO₃)₂ as a
320 function of molality concentration at 20-24 °C with a polynomial equation, and WSR were derived
321 to be 12.93, 16.12, 21.50 and 36.09 at 60, 70, 80 and 90% RH. As shown in Table 2, WSR were
322 measured to be 13.15±0.01, 16.30±0.01, 21.94±0.01 and 36.87±0.23 at 60, 70, 80 and 90% RH
323 for deliquesced Mg(NO₃)₂ at 25 °C. Therefore, it can be concluded that for WSR of Mg(NO₃)₂
324 solutions at ~25 °C, our work shows good agreement with the two previous studies (Ha and Chan,
325 1999; Rard et al., 2004).

326 **MgCl₂:** Water activities of MgCl₂ solutions were reported to be 0.909, 0.800, 0.692, 0.491
327 and 0.408 when the concentrations were 1.4, 2.4, 3.2, 4.6 and 5.2 mol kg⁻¹ (Rard and Miller, 1981),
328 i.e. WSR were equal to 10.7, 12.1, 17.4, 23.1 and 39.7 at 40.8, 49.1, 69.2, 80.0 and 90.9% RH. In
329 another work (Ha and Chan, 1999), an electrodynamic balance was used to investigate
330 hygroscopic growth of MgCl₂ particles at 20-24 °C, and the measured molality concentrations of
331 MgCl₂ solutions as a function of water activity were fitted by a polynomial equation. It can be
332 derived from Ha and Chen (1999) that WSR were equal to 10.65, 12.34, 14.29, 17.04, 22.24 and
333 34.78 when RH were 40, 50, 60, 70, 80 and 90%, respectively. WSR measured in our work, as
334 listed in Table 2, are 9.89±0.42, 11.52±0.48, 16.77±0.072, 16.74±0.72, 22.18±1.06 and 36.26±1.76
335 at 40, 50, 60, 70, 80 and 90% RH. As a result, our work agrees well with the two previous studies
336 (Rard and Miller, 1981; Ha and Chan, 1999) for WSR of MgCl₂ solutions as a function of RH at
337 ~25 °C.

338 **3.1.3 Phase transition of CaCl₂·xH₂O**

339 The change in sample mass of $\text{CaCl}_2 \cdot 6\text{H}_2\text{O}$ with RH was also investigated at 25 °C. As
340 shown in Figure 3, when dried at 0% RH, the sample mass was reduced by 1/3 (from ~1.5 to ~1.0),
341 and it is speculated that $\text{CaCl}_2 \cdot 6\text{H}_2\text{O}$ was converted to $\text{CaCl}_2 \cdot 2\text{H}_2\text{O}$. When RH was increased to
342 10%, no significant increase in sample mass was observed. As RH was further increased to 20%,
343 the sample mass was increased by 48 ± 7 %; this may indicate that $\text{CaCl}_2 \cdot 2\text{H}_2\text{O}$ was converted to
344 $\text{CaCl}_2 \cdot 6\text{H}_2\text{O}$, as the ratio of molar mass of $\text{CaCl}_2 \cdot 6\text{H}_2\text{O}$ (219 g mol^{-1}) to $\text{CaCl}_2 \cdot 2\text{H}_2\text{O}$ (147 g mol^{-1})
345 is 1.49, approximately equal to the ratio of sample mass at 20% RH to that at 10% RH. Further
346 increase in RH to 30% would lead to additional increase in sample mass, implying the
347 deliquescence of the sample and the formation of an aqueous CaCl_2 solution.



348
349 **Figure 3.** Change of normalized sample mass (blue curve, right y-axis) and RH (black curve, left
350 y-axis) as a function of time for $\text{CaCl}_2 \cdot x\text{H}_2\text{O}$ at 25 °C.

351

352 Assuming that $\text{CaCl}_2 \cdot 6\text{H}_2\text{O}$ was converted to $\text{CaCl}_2 \cdot 2\text{H}_2\text{O}$ after being dried at 0% RH, we
353 could use the change of sample mass as a function of RH to calculate WSR (defined as molar ratio
354 of H_2O to Ca^{2+}), and the results are listed in Table 3. Please note that we did not calculate WSR at
355 20% RH, since it is speculated that the significant mass increase at 20% RH was caused by the
356 transformation of $\text{CaCl}_2 \cdot 2\text{H}_2\text{O}$ to $\text{CaCl}_2 \cdot 6\text{H}_2\text{O}$, as mentioned above. Water activities of aqueous
357 CaCl_2 solutions as a function of molality concentration reported in a previous study (Rard et al.,
358 1977) were used to calculate WSR as a function of RH, and the results are also included in Table
359 3 for comparison. As evident from Table 3, at same/similar RH, WSR measured in our work are
360 in good agreement with those derived from Rard et al. (1977), supporting our assertion that
361 $\text{CaCl}_2 \cdot 6\text{H}_2\text{O}$ was converted to $\text{CaCl}_2 \cdot 2\text{H}_2\text{O}$ after being dried at 0% RH. In fact, theoretical
362 calculations (Kelly and Wexler, 2005) and experimental measurements (Gough et al., 2016) both
363 suggested that when RH is gradually increased, solid-solid phase transition from $\text{CaCl}_2 \cdot 2\text{H}_2\text{O}$ to
364 $\text{CaCl}_2 \cdot 6\text{H}_2\text{O}$ would occur before deliquescence takes place.

365
366 **Table 3.** Mass growth factors (m/m_0 , defined as the ratio of sample mass at a given RH to that at
367 0% RH) and water-to-solute ratios (WSR) as a function of RH (0-90%) at 25 °C for $\text{CaCl}_2 \cdot x\text{H}_2\text{O}$.
368 WSR derived from RH over aqueous CaCl_2 solutions as a function of concentration (mol kg^{-1}) at
369 25 °C (Rard et al., 1977) are also included for comparison. All the errors given in this work are
370 standard deviations.

our work			Rard et al., 1977		
RH (%)	m/m_0	WSR	RH (%)	molality	WSR
0	1.000±0.001	--	--	--	--
10	1.000±0.001	--	--	--	--
20	1.448±0.072	--	--	--	--
30	1.724±0.007	7.97±0.03	31.2	7.0	7.94

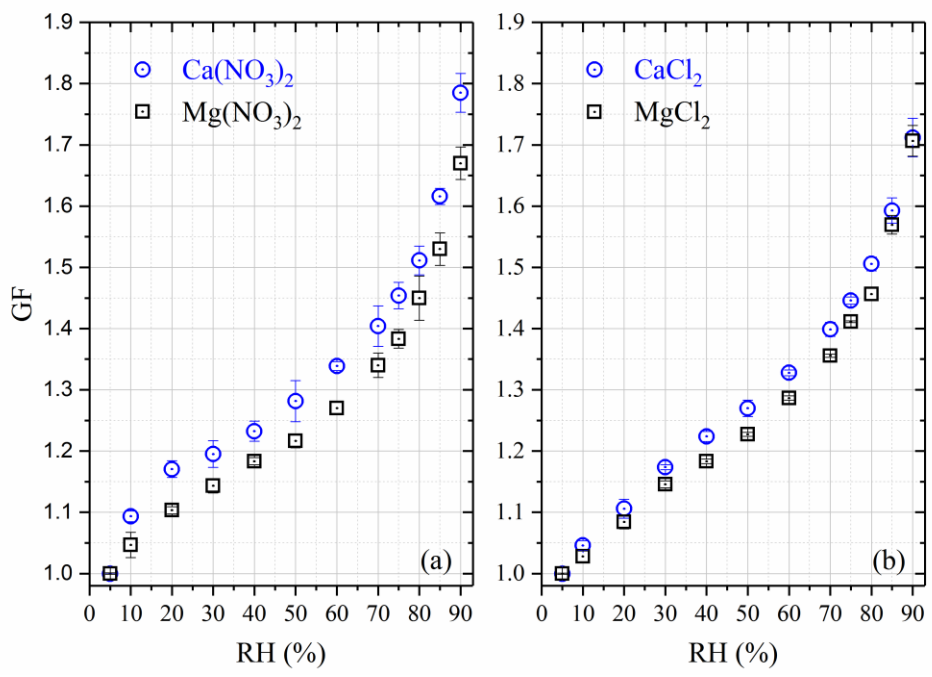
40	1.929±0.008	9.64±0.04	39.2	6.0	9.26
50	2.144±0.010	11.40±0.05	49.9	5.0	11.11
60	2.408±0.012	13.55±0.07	--	--	--
70	2.786±0.015	16.64±0.09	70.1	3.4	16.34
80	3.448±0.020	22.05±0.13	79.8	2.6	21.37
90	5.194±0.030	36.30±0.21	89.9	1.6	37.72

371

372 Additional experiments, in which RH was stepwise increased from 0% with an increment
373 of 1% per step, were carried out in attempt to measure the DRH of $\text{CaCl}_2 \cdot x\text{H}_2\text{O}$ at 25 °C. In all of
374 these experiments, $\text{CaCl}_2 \cdot 6\text{H}_2\text{O}$ was always transformed to $\text{CaCl}_2 \cdot 2\text{H}_2\text{O}$ after being dried at 0%
375 RH. In some of these experiments the deliquescence took place at RH of ~28.5%, which is
376 consistent with the DRH of $\text{CaCl}_2 \cdot 6\text{H}_2\text{O}$ reported in the literature (Kelly and Wexler, 2005),
377 suggesting that $\text{CaCl}_2 \cdot 2\text{H}_2\text{O}$ was first transformed to $\text{CaCl}_2 \cdot 6\text{H}_2\text{O}$ prior to deliquescence. However,
378 in some **other** experiments the deliquescence occurred at RH of ~18.5%, corresponding to the DRH
379 of $\text{CaCl}_2 \cdot 2\text{H}_2\text{O}$ reported previously (Kelly and Wexler, 2005), implying that $\text{CaCl}_2 \cdot 2\text{H}_2\text{O}$ was
380 deliquesced without being transformed to $\text{CaCl}_2 \cdot 6\text{H}_2\text{O}$. The dual deliquescence processes, i.e. 1)
381 transformation of $\text{CaCl}_2 \cdot 2\text{H}_2\text{O}$ to $\text{CaCl}_2 \cdot 6\text{H}_2\text{O}$ prior to deliquescence and 2) direct deliquescence
382 of $\text{CaCl}_2 \cdot 2\text{H}_2\text{O}$, were also observed using Raman spectroscopy at low temperatures (223-273 K)
383 (Gough et al., 2016). It seems that the competition of these two mechanisms are both
384 thermodynamically and kinetically dependent. Since phase transitions of CaCl_2 are not only
385 important for atmospheric aerosols but may also play a role in the existence of liquid water in some
386 hyperarid environments (Gough et al., 2016), further investigation is being carried out by
387 combining the vapor sorption analyzer technique with vibrational spectroscopy.

388 3.1.4 Hygroscopic growth of aerosol particles

389 Hygroscopic growth factors (GF), which were measured using H-TDMA at room
 390 temperature, are displayed in Figure 4 for $\text{Ca}(\text{NO}_3)_2$, CaCl_2 , $\text{Mg}(\text{NO}_3)_2$ and MgCl_2 aerosols, and
 391 the results are also compiled in Table 4. It was found in our work that all the four types of aerosols
 392 exhibit high hygroscopicity, with GF at 90% RH being around 1.7 or larger. In addition, all the
 393 four types of aerosol particles, instead of having distinct solid-liquid phase transitions, showed
 394 significant hygroscopic growth at very low RH (as low as 10%), and their GF increased
 395 continuously with RH. This phenomenon is due to the fact that these aerosol particles, generated
 396 by drying aqueous droplets, were likely to be amorphous. It was also observed in previous work
 397 that some types of particles generated by drying aqueous droplets would be amorphous, such as
 398 $\text{Ca}(\text{NO}_3)_2$ (Tang and Fung, 1997; Gibson et al., 2006; Jing et al., 2018), $\text{Mg}(\text{NO}_3)_2$ (Zhang et al.,
 399 2004; Gibson et al., 2006; Li et al., 2008a), CaCl_2 (Park et al., 2009; Tobo et al., 2009) and MgCl_2
 400 (Cziczo and Abbatt, 2000; Park et al., 2009).



401
 402 **Figure 4.** Hygroscopic growth factors (GF) of aerosol particles as a function of RH measured
 403 using H-TDMA. (a): $\text{Ca}(\text{NO}_3)_2$ and $\text{Mg}(\text{NO}_3)_2$; (b) CaCl_2 and MgCl_2 .

404
405
406
407
408
409
410
411
412
413
414
415
416
417
418
419
420
421

Ca(NO₃)₂ and Mg(NO₃)₂ aerosols: Two previous studies (Gibson et al., 2006; Jing et al., 2018) employed H-TDMA to examine hygroscopic growth of 100 nm Ca(NO₃)₂ aerosol particles at room temperature. GF were determined to be 1.51 at 80% RH and ~1.77 at 85% RH by Gibson et al. (2008). It should be pointed out that though the DMA-selected dry particle diameters were 100 nm for Ca(NO₃)₂ and Mg(NO₃)₂ aerosols, the dry diameters used by Gibson et al. (2006) were 89 nm for Ca(NO₃)₂ and 77 nm for Mg(NO₃)₂, being extrapolated to 0% RH using the theoretical growth curve based on the Köhler theory. The Köhler theory is based on assumption of solution ideality, and thus may not be applicable to highly concentrated aerosol droplets at low RH (Seinfeld and Pandis, 2016). If the dry diameter selected using the DMA (i.e. 100 nm) was used in GF calculation, GF reported by Gibson et al. (2006) would be ~1.34 at 80% RH and ~1.58 at 85% RH; compared with our results (1.51±0.02 at 80% RH and 1.62±0.01 at 85% RH), GF reported by Gibson et al. (2006) are ~11% smaller at 80% RH and only ~3% smaller at 85%. In the second study (Jing et al., 2018), GF were determined to be 1.56 at 80% RH and 1.89 at 90% RH; compared with our results (1.51±0.02 at 80% RH and 1.79±0.03 at 90% RH), GF reported by Jing et al. (2018) were ~3% larger at 80% RH and ~6% larger at 90% RH. Overall, our results show reasonably good agreement with the two previous studies (Gibson et al., 2006; Jing et al., 2018).

Table 4. Hygroscopic growth factors (GF) of Ca(NO₃)₂, CaCl₂, Mg(NO₃)₂ and MgCl₂ aerosol particles measured at room temperature using H-TDMA. The absolute uncertainties in RH were estimated to be within ±2%. All the errors given in this work are standard deviations.

RH (%)	Ca(NO ₃) ₂	CaCl ₂	Mg(NO ₃) ₂	MgCl ₂
<5	1.00±0.01	1.00±0.01	1.00±0.01	1.00±0.01
10	1.09±0.01	1.05±0.01	1.05±0.02	1.03±0.01

20	1.17±0.02	1.11±0.02	1.10±0.01	1.08±0.01
30	1.20±0.02	1.17±0.01	1.41±0.01	1.15±0.01
40	1.23±0.02	1.22±0.01	1.18±0.01	1.18±0.01
50	1.28±0.03	1.27±0.01	1.22±0.01	1.23±0.01
60	1.34±0.01	1.33±0.01	1.27±0.01	1.29±0.01
70	1.40±0.03	1.40±0.01	1.34±0.02	1.36±0.01
75	1.45±0.02	1.45±0.01	1.38±0.02	1.41±0.01
80	1.51±0.02	1.51±0.01	1.45±0.04	1.46±0.01
85	1.62±0.01	1.59±0.02	1.53±0.03	1.57±0.02
90	1.79±0.03	1.71±0.03	1.67±0.03	1.71±0.03

425

426 To our knowledge, only one previous study investigated the hygroscopic growth of
427 $\text{Mg}(\text{NO}_3)_2$ aerosol (100 nm) using the H-TDMA (Gibson et al., 2006), and GF was measured to
428 be 1.94 ± 0.02 at 83% RH. As stated above, the theoretical extrapolated diameter (77 nm) at 0%
429 RH, instead of the dry diameter (100 nm) selected using the DMA, were used as the dry diameter
430 to calculate their reported GF (Gibson et al., 2006). If the DMA-selected dry diameter (100 nm)
431 was used in calculation, the GF reported by Gibson et al. (2006) would be ~ 1.49 at 83% RH; for
432 comparison, in our work GF were determined to be 1.45 ± 0.04 and 1.53 ± 0.03 at 80 and 85% RH,
433 suggesting good agreement between the two studies if the DMA-selected dry diameter was used
434 to calculate GF reported by Gibson et al. (2006).

435 **CaCl₂ and MgCl₂ aerosols:** Hygroscopic growth of CaCl₂ and MgCl₂ aerosol particles
436 was explored using a H-TDMA (Park et al., 2009), and as far as we know, this was the only study
437 which reported the H-TDMA measured hygroscopic growth factors of the two **types of** aerosols.
438 Three dry diameters (20, 30 and 50 nm) were used for CaCl₂ and MgCl₂ aerosol particles (Park et
439 al., 2009), and no significant size dependence of their hygroscopic properties was observed. GF
440 were measured to be around 1.27, 1.38, 1.48 and 1.59 at 60, 75, 80 and 90 % RH for CaCl₂ (Park

441 et al., 2009). For comparison, GF were determined in this work to be 1.33 ± 0.01 , 1.45 ± 0.01 ,
442 1.51 ± 0.01 and 1.71 ± 0.03 at 60, 75, 80 and 90 %, slightly larger than those reported by Park et al.
443 (2009), and the differences were found to be $<7\%$.

444 At 50, 70, 80, 85 and 90% RH, GF of MgCl_2 aerosol were measured to be about 1.17, 1.29,
445 1.47, 1.59 and 1.79 by Park et al. (2009); for comparison, GF were determined to be 1.23 ± 0.01 ,
446 1.36 ± 0.01 , 1.46 ± 0.01 , 1.57 ± 0.02 and 1.71 ± 0.03 in our work at the same RHs. The differences did
447 not exceed 6% **at any given RH**, suggesting good agreement between the two studies. Microscopy
448 was used to investigate the hygroscopic growth of micrometer-size MgCl_2 particles deposited on
449 substrates (Gupta et al., 2015), and the ratios of 2-D particle areas, relative to that at $<5\%$ RH,
450 were measured to be around 1.65, 1.92, 2.02 and 2.28 at 60, 70, 75 and 80% RH, corresponding to
451 diameter-based GF of approximately 1.28, 1.38, 1.42 and 1.51, respectively. GF of MgCl_2 aerosol,
452 as shown in Table 4, were determined to be 1.29 ± 0.01 , 1.36 ± 0.01 , 1.41 ± 0.01 and 1.46 ± 0.01 at 60,
453 70, 75 and 80% RH in our work; therefore, the differences between GF reported in our work and
454 those measured by Gupta et al. (2015) were $<4\%$.

455 **Comparison between hygroscopic growth with CCN activities:** GF measured using H-
456 TDMA can be used to calculate the single hygroscopicity parameter, κ_{gf} , using Eq. (3a) (Petters
457 and Kreidenweis, 2007; Kreidenweis and Asa-Awuku, 2014; Tang et al., 2016a):

458
$$\frac{RH}{\exp\left(\frac{A_k}{d_0 \cdot GF}\right)} = \frac{GF^3 - 1}{GF^3 - (1 - \kappa_{gf})} \quad (3a)$$

459 where GF is the growth factor at a given RH; A_k is a constant which describes the Kelvin effect
460 and is equal to 2.1 nm for a surface tension of 0.072 J m^{-2} (pure water) and temperature of 298.15
461 K (Tang et al., 2016a). For a dry particle diameter (d_0) of 100 nm, the denominator in the left term

462 of Eq. (3a) is not larger than 1.02; therefore, the Kelvin effect is negligible and Eq. (3a) can be
463 simplified to Eq. (3b):

$$464 \quad RH = \frac{GF^3 - 1}{GF^3 - (1 - \kappa_{gf})} \quad (3b)$$

465 Eq. (4) can be derived by rearranging Eq. (3b):

$$466 \quad \kappa_{gf} = (GF^3 - 1) \frac{1 - RH}{RH} \quad (4)$$

467 In our work, GF data at 90% RH were used to derive κ_{gf} , as usually done in many previous studies
468 (Kreidenweis and Asa-Awuku, 2014). The single hygroscopicity parameter, κ_{ccn} , can also be
469 derived from experimental measurements or theoretical calculations of CCN activities (Petters and
470 Kreidenweis, 2007; Kreidenweis and Asa-Awuku, 2014). Ideally aerosol-water interactions under
471 both subsaturation and supersaturation can be described by a constant single hygroscopicity
472 parameter (Petters and Kreidenweis, 2007). Nevertheless, agreement and discrepancies between
473 growth factors derived and CCN activity derived κ have been reported (Petters and Kreidenweis,
474 2007; Petters et al., 2009; Wex et al., 2009), and several factors can contribute to such
475 discrepancies. First of all, the solutions may not be ideal, and especially aerosol particles under
476 subsaturation may consist of concentrated solutions; secondly, some of the compounds may have
477 limited solubilities. As discussed previously (Petters and Kreidenweis, 2007; Prenni et al., 2007),
478 both factors would lead to lower κ_{gf} , compared to κ_{ccn} . The effect of reduced surface tension,
479 compared to pure water, should be negligible for the eight types of aerosol particles considered in
480 our work, since none of these compounds are known to be surface-active.

481 Comparison between κ_{gf} determined in our work and κ_{ccn} measured in previous studies is
482 summarized in Table 5 and discussed below for $\text{Ca}(\text{NO}_3)_2$, CaCl_2 , $\text{Mg}(\text{NO}_3)_2$ and MgCl_2 aerosols.
483 In previous work which measured CCN activities (Sullivan et al., 2009; Tang et al., 2015; Gaston

484 et al., 2017), the dry particle diameters used were typically in the range of 50-125 nm. The
 485 uncertainties in our derived κ_{gf} have taken into account the uncertainties in measured GF at 90%
 486 RH.

487

488 **Table 5.** Comparison between κ_{gf} measured in our work and κ_{ccn} measured in previous studies.

aerosol	κ_{gf} (this work)	κ_{ccn} (previous studies)
Ca(NO ₃) ₂	0.49-0.56	0.44-0.64 (Sullivan et al., 2009) 0.57-0.59 (Tang et al., 2015)
Mg(NO ₃) ₂	0.38-0.43	not measured yet
CaCl ₂	0.42-0.47	0.46-0.58 (Sullivan et al, 2009) 0.51-0.54 (Tang et al, 2015)) 0.549-0.561 (Gaston et al., 2017)
MgCl ₂	0.42-0.47	0.456-0.464 (Gaston et al., 2017)
Ca(HCOO) ₂	0.28-0.31	0.47-0.52 (Tang et al., 2015)
Mg(HCOO) ₂	0.40-0.45	not measured yet
Ca(CH ₃ COO) ₂	0.09-0.13	0.37-0.47 (Tang et al., 2015)
Mg(CH ₃ COO) ₂	0.28-0.29	not measured yet

489

490 1) For Ca(NO₃)₂ aerosol, κ_{ccn} were measured to be 0.44-0.64 by Sullivan et al. (2009) and
 491 0.57-0.59 by Tang et al. (2015); in our work GF at 90% RH was measured to be 1.79 ± 0.03 , giving
 492 κ_{gf} of 0.49-0.56, in good agreement with κ_{ccn} reported by the two previous studies (Sullivan et al.,
 493 2009; Tang et al., 2015).

494 2) For CaCl₂ aerosol, κ_{ccn} were measured to be 0.46-0.58 by Sullivan et al. (2009), 0.51-
 495 0.54 by Tang et al. (2015), and 0.549-0.561 by Gaston et al. (2017). GF at 90% RH was determined
 496 to be 1.71 ± 0.03 in present work, giving κ_{gf} of 0.42-0.47, slightly lower than κ_{ccn} values measured
 497 previously (Sullivan et al., 2009; Tang et al., 2015; Gaston et al., 2017).

498 3) In our work, GF was determined to be 1.71 ± 0.03 for MgCl_2 at 90% RH, giving κ_{gf} of
499 0.42-0.47; a previous study (Gaston et al., 2017) measured the CCN activity of MgCl_2 aerosol, and
500 κ_{ccn} were determined to be 0.456-0.464, in good agreement with κ_{gf} measured in our work.

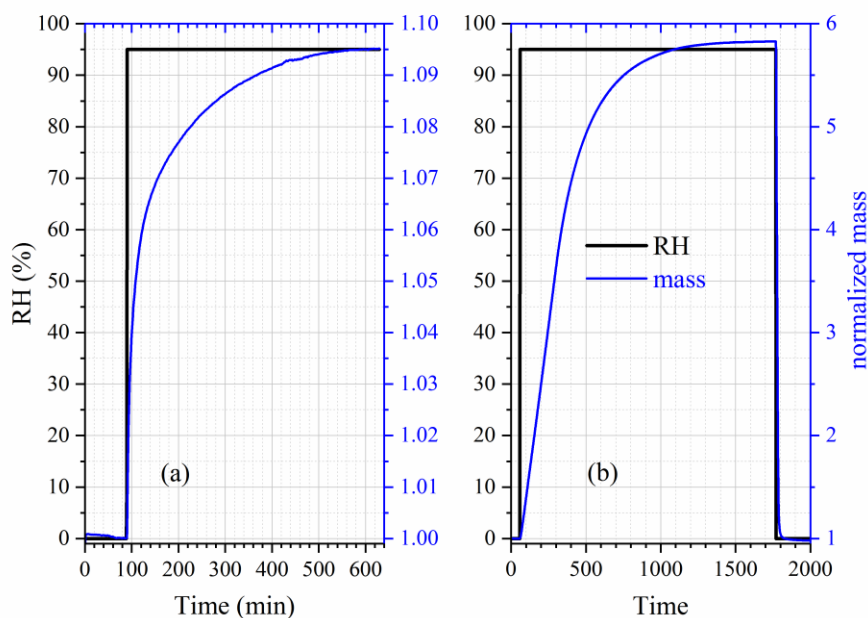
501 4) For $\text{Mg}(\text{NO}_3)_2$ aerosol, GF and κ_{gf} were determined in our work to be 1.67 ± 0.03 and
502 0.38-0.43, respectively. To our knowledge, CCN activities of $\text{Mg}(\text{NO}_3)_2$ aerosol have not been
503 experimentally explored yet, and κ_{ccn} were predicted to be 0.8 for $\text{Mg}(\text{NO}_3)_2$ and 0.3 for
504 $\text{Mg}(\text{NO}_3)_2 \cdot 6\text{H}_2\text{O}$ (Kelly et al., 2007; Kreidenweis and Asa-Awuku, 2014), exhibiting a large
505 variation for the same compound with different hydrate states under dry conditions. These
506 calculations were performed using the Köhler theory, assuming solution ideality (Kelly et al.,
507 2007). As Kelly et al. (2007) pointed out, the hydration states, which are not entirely clear for
508 $\text{Mg}(\text{NO}_3)_2$ aerosol particles under atmospherically relevant conditions, can have large impacts on
509 their hygroscopicity and CCN activities.

510 **3.2 Hygroscopicity of formates and acetates**

511 **3.2.1 DRH and water-to-solute ratios**

512 We measured the mass change of $\text{Ca}(\text{HCOO})_2$, $\text{Mg}(\text{HCOO})_2 \cdot 2\text{H}_2\text{O}$ and
513 $\text{Ca}(\text{CH}_3\text{COO})_2 \cdot \text{H}_2\text{O}$ samples as a function of RH at 25 °C, and found that the sample mass
514 remained essentially constant for all the three compounds when RH was increased from 0 to 90%.
515 Therefore, a series of experiments in which RH was increased to 95% were conducted, and for
516 each compounds three duplicate experiments were carried out. As shown in Figure 5a, when RH
517 was increased from 0 to 95%, a significant while small increase in sample mass (~10%) was
518 observed for $\text{Ca}(\text{HCOO})_2$. The average ratio of sample mass at 95% RH to that at 0% RH was
519 determined to be for 1.119 ± 0.036 for $\text{Ca}(\text{HCOO})_2$ and 1.064 ± 0.020 for $\text{Mg}(\text{HCOO})_2 \cdot 2\text{H}_2\text{O}$ (not

520 shown in Figure 5), probably indicating that the DRH values were >95% for both compounds at
521 25 °C.



522
523 **Figure 5.** Change of normalized sample mass (blue curve, right y-axis) and RH (black curve, left
524 y-axis) as a function of time at 25 °C. (a) Ca(HCOO)₂; (b) Ca(CH₃COO)₂·H₂O.

525
526 When RH was increased from 0 to 95%, large increase in sample mass (almost by a factor
527 of 6), as shown in Figure 6b, was observed for Ca(CH₃COO)₂·H₂O. On average, the ratio of sample
528 mass at 95% RH to that at 0% RH was measured to be 5.849±0.064, corresponding to a WSR
529 (defined as the molar ratio of H₂O to Ca²⁺) of 48.42±0.53 for the aqueous Ca(CH₃COO)₂ solution
530 at 95% RH. This observation suggested that the deliquescence of Ca(CH₃COO)₂·H₂O at 25 °C
531 occurred between 90 and 95% RH. In further experiments significant increase in sample mass
532 (by >10%, and the sample was still increasing sharply when the experiment was terminated) was
533 observed when RH was increased from 90 to 91% for Ca(CH₃COO)₂·H₂O at 25 °C, suggesting a
534 measured DRH of 90.5±1.0 %. The DRH of Ca(CH₃COO)₂ and internally mixed

535 $\text{CaCO}_3/\text{Ca}(\text{CH}_3\text{COO})_2$ particles were measured to be 85 and 88% at 5 °C (Ma et al., 2012), using
 536 a modified physisorption analyzer. Since in these two studies DRH were measured at different
 537 temperatures (25 °C in our work and 5 °C by Ma et al.) and the absolute difference in reported
 538 DRH was ~5%, the agreement in reported DRH can be considered to be quite good for
 539 $\text{Ca}(\text{CH}_3\text{COO})_2$.

540 Table 6 summarizes the ratios of sample mass at a given RH to that at 0% RH for
 541 $\text{Mg}(\text{CH}_3\text{COO})_2 \cdot 4\text{H}_2\text{O}$ as a function of RH at 25°C. Being different from $\text{Ca}(\text{HCOO})_2$,
 542 $\text{Mg}(\text{HCOO})_2 \cdot 2\text{H}_2\text{O}$ and $\text{Ca}(\text{CH}_3\text{COO})_2 \cdot \text{H}_2\text{O}$, large increase in sample mass was observed for
 543 $\text{Mg}(\text{CH}_3\text{COO})_2 \cdot 4\text{H}_2\text{O}$ when RH was increased from 70 to 80%. This observation suggested that
 544 the deliquescence of $\text{Mg}(\text{CH}_3\text{COO})_2 \cdot 4\text{H}_2\text{O}$ occurred between 70 and 80% RH. Further
 545 experiments were carried out to measure its DRH, and significant increase in sample mass occurred
 546 when RH was increased from 71 to 72%, giving a measured DRH of $71.5 \pm 1.0\%$ at 25 °C. The RH
 547 over the saturated $\text{Mg}(\text{CH}_3\text{COO})_2$ solution at ~23 °C was measured to be 65% (Wang et al., 2005),
 548 slightly lower than the DRH determined in our work.

549
 550 **Table 6.** Mass growth factors (m/m_0 , defined as the ratios of sample mass at a given RH to that at
 551 0% RH) and water-to-solute ratios (WSR) as a function of RH (0-90%) at 25 °C for
 552 $\text{Mg}(\text{CH}_3\text{COO})_2 \cdot 4\text{H}_2\text{O}$. WSR are only calculated for RH exceeding the DRH (i.e. when the sample
 553 was deliquesced). All the errors given in this work are standard deviations.

RH (%)	0	10	20	30	40
m/m_0	1.000±0.001	1.012±0.021	1.012 ±0.022	1.013 ±0.022	1.013±0.022
WSR	--	--	--	--	--
RH (%)	50	60	70	80	90
m/m_0	1.014±0.023	1.015±0.025	1.033±0.031	2.029±0.013	3.100±0.021
WSR	--	--	--	16.24±0.11	28.97±0.20

554

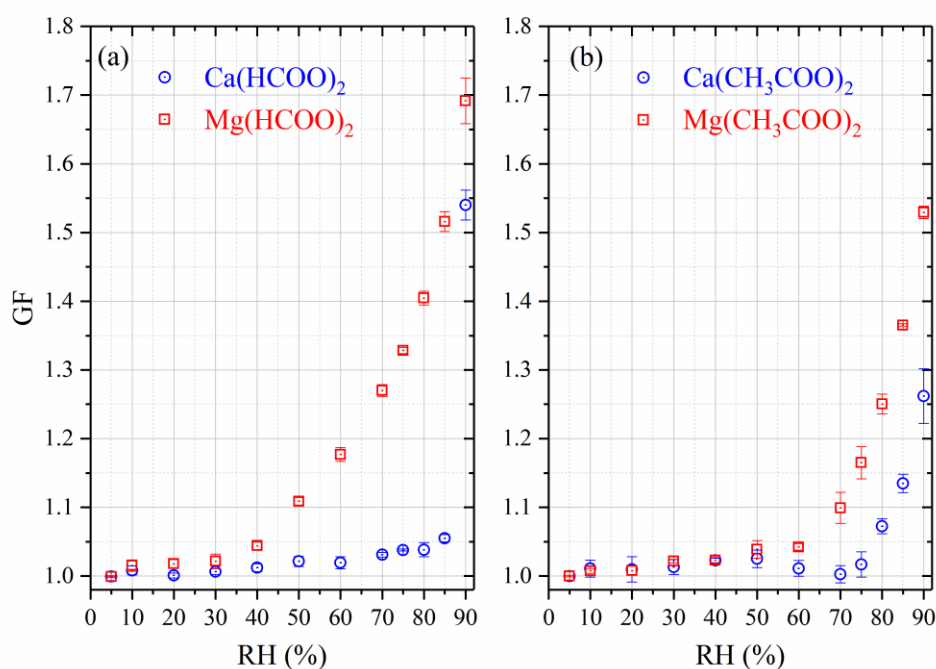
555 The ratios of sample mass, relative to that at 0% RH, were measured to be 2.029 ± 0.013
556 and 3.100 ± 0.021 at 80 and 90% RH, corresponding to WSR of 16.24 ± 0.11 at 80% RH and
557 28.97 ± 0.20 at 90% RH for aqueous $\text{Mg}(\text{CH}_3\text{COO})_2$ solutions. A electrodynamic balance coupled
558 to Raman spectroscopy was employed to study the hygroscopic growth of $\text{Mg}(\text{CH}_3\text{COO})_2$ at ~ 23
559 $^\circ\text{C}$ (Wang et al., 2005), and WSR was determined to be ~ 15.6 at 80% RH, in good agreement with
560 our work. Ma et al. (2012) found that after heterogeneous reaction with $\text{CH}_3\text{COOH}(\text{g})$ at 50% RH
561 for 12 h, the hygroscopicity of MgO particles, which was initially rather non-hygroscopic, was
562 substantially increased due to the formation of $\text{Mg}(\text{CH}_3\text{COO})_2$. The conclusion drawn by Ma et al.
563 (2012) is qualitatively consistent with the results obtained in our work.

564 Table 6 also reveals that a small increase in sample mass (by $\sim 3\%$, relative to that at 0%
565 RH) was observed for $\text{Mg}(\text{CH}_3\text{COO})_2 \cdot 4\text{H}_2\text{O}$ when RH was increased to 70% before the
566 deliquescence of $\text{Mg}(\text{CH}_3\text{COO})_2 \cdot 4\text{H}_2\text{O}$ took place. This could be due to the possibility that
567 $\text{Mg}(\text{CH}_3\text{COO})_2 \cdot 4\text{H}_2\text{O}$ samples used in our work may contain a small fraction of amorphous
568 $\text{Mg}(\text{CH}_3\text{COO})_2$, which would take up some amount of water at RH below the DRH of
569 $\text{Mg}(\text{CH}_3\text{COO})_2 \cdot 4\text{H}_2\text{O}$ (Wang et al., 2005; Pang et al., 2015).

570 **3.2.2 Hygroscopic growth of aerosol particles**

571 Figure 6 and Table 7 display hygroscopic growth factors of $\text{Ca}(\text{HCOO})_2$, $\text{Mg}(\text{HCOO})_2$,
572 $\text{Ca}(\text{CH}_3\text{COO})_2$ and $\text{Mg}(\text{CH}_3\text{COO})_2$ aerosols, measured in our work using H-TDMA. To the best
573 of our knowledge, this is the first time that GF of these four types of aerosols have been reported.
574 For $\text{Mg}(\text{HCOO})_2$, aerosol particles showed gradual while small growth for RH up to 30%, and
575 further increase in RH led to significant growth; the average GF of $\text{Mg}(\text{HCOO})_2$ aerosol at 90%
576 RH was determined to be 1.69 ± 0.03 , similar to those for $\text{Mg}(\text{NO}_3)_2$ (1.67 ± 0.03) and MgCl_2

577 (1.71±0.03) at the same RH. For RH up to 85%, Ca(HCOO)₂ aerosol particles exhibited gradual
 578 and small growth; when RH was increased to 90%, abrupt and large growth was observed, with
 579 GF being 1.54±0.02, significantly smaller than that for Mg(HCOO)₂ aerosol at the same RH. This
 580 is distinctively different from what was observed in VSA experiments, in which the mass of
 581 Ca(HCOO)₂ and Mg(HCOO)₂·2H₂O powdered samples was only increased by ~12% and ~6%
 582 when RH was increased from 0 to 95%. This difference may be explained by different states of
 583 samples used in these two types of experiments (i. e. crystalline samples in VSA experiments,
 584 while likely amorphous aerosol particles in H-TDMA measurements), leading to different
 585 hygroscopic behaviors.



586
 587 **Figure 6.** Hygroscopic growth factors (GF) of aerosol particles as a function of RH measured
 588 using H-TDMA. (a): Ca(HCOO)₂ and Mg(HCOO)₂; (b) Ca(CH₃COO)₂ and Mg(CH₃COO)₂.

589
 590 As shown in Figure 6b, gradual and small growth was also observed for Ca(CH₃COO)₂
 591 and Mg(CH₃COO)₂ aerosols at low RH. Fast increase in GF started at about 80% RH for

592 $\text{Ca}(\text{CH}_3\text{COO})_2$ aerosol, and the GF was determined to be 1.26 ± 0.04 at 90% RH. As discussed in
593 Section 3.2.1, in VSA experiments no significant increase in sample mass was observed for
594 $\text{Ca}(\text{CH}_3\text{COO})_2\cdot\text{H}_2\text{O}$ when RH was increased from 0 to 90%, being different from H-TDMA results.
595 This difference may again be explained (at least partly) by different states of particles used in these
596 two types of experiments, as mentioned above. Careful inspection of Figure 6b and Table 7 reveals
597 that a small decrease in GF from 1.03 ± 0.01 to 1.00 ± 0.01 for $\text{Ca}(\text{CH}_3\text{COO})_2$ aerosol when RH was
598 increased from 50 to 70%. The decrease in GF may be caused by restructuring of particles or
599 change in particle morphology (Vlasenko et al., 2005; Koehler et al., 2009); in addition, the small
600 change in GF (~ 0.03) may not be significant when compared to the uncertainties in our H-TDMA
601 measurements.

602 When RH increased from 0 to 70%, small and gradual growth occurred for $\text{Mg}(\text{CH}_3\text{COO})_2$
603 aerosol particles, indicating that these particles may contain some amount of amorphous materials.
604 It was also found in previous work (Li et al., 2008a; Li et al., 2008b) that $\text{Mg}(\text{NO}_3)_2$ particles
605 generated by drying aqueous droplets were amorphous. Figure 6b reveals that further increase in
606 RH led to large increase in growth factors, and this is largely consistent with the occurrence of
607 deliquescence at $\sim 71.5\%$ RH at 25 °C for $\text{Mg}(\text{CH}_3\text{COO})_2\cdot 4\text{H}_2\text{O}$, as mentioned in Section 3.2.1. At
608 90% RH, GF of $\text{Mg}(\text{CH}_3\text{COO})_2$ aerosol was determined to be 1.53 ± 0.01 , much larger than that for
609 $\text{Ca}(\text{CH}_3\text{COO})_2$ (1.26 ± 0.04).

610 At 90% RH, for the four Ca-containing salts considered in our study, nitrate and chloride
611 aerosols have very similar GF (1.79 ± 0.03 versus 1.71 ± 0.03), which are large than that of formate
612 (1.54 ± 0.02), and acetate has the smallest GF (1.26 ± 0.04). For comparison, the variation in GF at
613 90% RH was found to be considerably smaller (from ~ 1.53 to ~ 1.71) for the four Mg-containing
614 salts studied herein.

615

616 **Table 7.** Hygroscopic growth factors of $\text{Ca}(\text{HCOO})_2$, $\text{Ca}(\text{CH}_3\text{COO})_2$, $\text{Mg}(\text{HCOO})_2$ and
 617 $\text{Mg}(\text{CH}_3\text{COO})_2$ aerosol particles measured using H-TDMA. The absolute uncertainties in RH were
 618 estimated to be within $\pm 2\%$. All the errors given in this work are standard deviations.

RH (%)	$\text{Ca}(\text{HCOO})_2$	$\text{Ca}(\text{CH}_3\text{COO})_2$	$\text{Mg}(\text{HCOO})_2$	$\text{Mg}(\text{CH}_3\text{COO})_2$
5	1.00 \pm 0.01	1.00 \pm 0.01	1.00 \pm 0.01	1.00 \pm 0.01
10	1.01 \pm 0.01	1.01 \pm 0.01	1.02 \pm 0.01	1.01 \pm 0.01
20	1.01 \pm 0.01	1.01 \pm 0.02	1.02 \pm 0.01	1.01 \pm 0.01
30	1.01 \pm 0.01	1.01 \pm 0.01	1.02 \pm 0.01	1.02 \pm 0.01
40	1.01 \pm 0.01	1.02 \pm 0.01	1.04 \pm 0.01	1.02 \pm 0.01
50	1.02 \pm 0.01	1.03 \pm 0.01	1.11 \pm 0.01	1.04 \pm 0.01
60	1.02 \pm 0.01	1.01 \pm 0.01	1.18 \pm 0.01	1.04 \pm 0.01
70	1.03 \pm 0.01	1.00 \pm 0.01	1.27 \pm 0.01	1.10 \pm 0.02
75	1.04 \pm 0.01	1.02 \pm 0.02	1.33 \pm 0.01	1.16 \pm 0.02
80	1.04 \pm 0.01	1.07 \pm 0.01	1.41 \pm 0.01	1.25 \pm 0.01
85	1.01 \pm 0.01	1.13 \pm 0.01	1.52 \pm 0.02	1.37 \pm 0.01
90	1.54 \pm 0.02	1.26 \pm 0.04	1.69 \pm 0.03	1.53 \pm 0.01

619

620 According to Eq. (4), GF measured at 90% RH can be used to calculate κ_{gf} , which were
 621 determined to be 0.28-0.31 for $\text{Ca}(\text{HCOO})_2$, 0.09-0.13 for $\text{Ca}(\text{CH}_3\text{COO})_2$, 0.40-0.45 for
 622 $\text{Mg}(\text{HCOO})_2$, and 0.28-0.29 for $\text{Mg}(\text{CH}_3\text{COO})_2$. A previous study (Tang et al., 2015) investigated
 623 the CCN activities of $\text{Ca}(\text{HCOO})_2$ and $\text{Ca}(\text{CH}_3\text{COO})_2$ aerosols and reported their single
 624 hygroscopicity parameters (κ_{ccn}), while the CCN activities of $\text{Mg}(\text{HCOO})_2$ and $\text{Mg}(\text{CH}_3\text{COO})_2$
 625 have not been explored yet. As summarized in Table 5, κ_{ccn} was reported to be 0.47-0.52 for
 626 $\text{Ca}(\text{HCOO})_2$ (Tang et al., 2015), significantly larger than κ_{gf} (0.28-0.31) determined in our work;
 627 for $\text{Ca}(\text{CH}_3\text{COO})_2$, Tang et al. (2015) reported κ_{ccn} to be in the range of 0.37-0.47, again much
 628 larger than κ_{gf} (0.09-0.13) derived from the present work.

629 As discussed in Section 3.1.4, for $\text{Ca}(\text{NO}_3)_2$ and CaCl_2 aerosols, κ_{gf} derived from H-TDMA
630 experiments in the present work show fairly good agreement with κ_{ccn} derived from CCN activities
631 measured in previous studies (Sullivan et al., 2009; Tang et al., 2015); in contrast, for $\text{Ca}(\text{HCOO})_2$
632 and $\text{Ca}(\text{CH}_3\text{COO})_2$ aerosols, κ_{gf} derived from our H-TDMA experiments are significantly smaller
633 than κ_{ccn} reported by the previous study (Tang et al., 2015). This can be largely caused by the
634 difference in water solubilities of $\text{Ca}(\text{NO}_3)_2$, CaCl_2 , $\text{Ca}(\text{HCOO})_2$ and $\text{Ca}(\text{CH}_3\text{COO})_2$.
635 $\text{Ca}(\text{NO}_3)_2 \cdot 4\text{H}_2\text{O}$ and $\text{CaCl}_2 \cdot 6\text{H}_2\text{O}$, with solubilities being 1983 and 1597 g per kg water at 25 °C
636 (Kelly and Wexler, 2005), can be considered to be highly soluble; for comparison, the solubilities
637 were reported to be 166 g per kg water for $\text{Ca}(\text{HCOO})_2$ at 25 °C and 347 g per kg water for
638 $\text{Ca}(\text{CH}_3\text{COO})_2 \cdot 2\text{H}_2\text{O}$ at 20 °C (Dean, 1973). Due to their limited water solubilities, $\text{Ca}(\text{HCOO})_2$
639 and $\text{Ca}(\text{CH}_3\text{COO})_2$ aerosol particles may not be fully dissolved at 90% RH in the H-TDMA
640 experiments but would be dissolved to a larger extent (if not completely) for RH >100% in CCN
641 activity measurements (Petters and Kreidenweis, 2008; Kreidenweis and Asa-Awuku, 2014).
642 Therefore, for $\text{Ca}(\text{HCOO})_2$ and $\text{Ca}(\text{CH}_3\text{COO})_2$ aerosols, κ_{gf} derived from H-TDMA measurements
643 would be smaller than κ_{ccn} derived from CCN activity measurements. In fact, the observation that
644 κ_{gf} appeared to be significantly smaller than κ_{ccn} , largely caused by limited water solubilities of
645 compounds under investigation, has been well documented in the literature for laboratory-
646 generated and ambient aerosol particles (Chang et al., 2007; Prenni et al., 2007; Wex et al., 2009;
647 Good et al., 2010; Massoli et al., 2010).

648 **3.3 Discussion**

649 **3.3.1 Comparison between H-TDMA and VSA measurements**

650 In this work two complementary techniques were employed to investigate hygroscopic
651 properties of Ca- and Mg-containing compounds. The mass change of bulk samples was measured

652 as a function of RH using VSA, and the change in aerosol diameter with RH was determined using
653 H-TDMA. Two major questions can be asked regarding the results obtained using the two different
654 techniques: 1) How can the two types of results be reconciled? 2) What is the atmospheric
655 relevance of each type of results? Below we use $\text{Ca}(\text{NO}_3)_2$ at room temperature as an example for
656 discussion, and similar conclusions can be drawn for the other seven compounds.

657 As presented in Section 3.1, at 25 °C the deliquescence of $\text{Ca}(\text{NO}_3)_2 \cdot 4\text{H}_2\text{O}$ took place at
658 52-53% RH. In contrast, dry $\text{Ca}(\text{NO}_3)_2$ aerosol particles generated by atomizing aqueous solutions
659 were likely to be amorphous (Tang and Fung, 1997; Al-Abadleh et al., 2003; Gibson et al., 2006);
660 as a result, they exhibited continuous hygroscopic growth with increasing RH with no distinct
661 solid-liquid phase transitions observed. When RH exceed the DRH of $\text{Ca}(\text{NO}_3)_2 \cdot 4\text{H}_2\text{O}$, both
662 $\text{Ca}(\text{NO}_3)_2 \cdot 4\text{H}_2\text{O}$ bulk samples and $\text{Ca}(\text{NO}_3)_2$ aerosol particles are expected to deliquesce to form
663 aqueous solutions. To directly link the mass change (measured using VSA) with diameter change
664 (measured using H-TDMA), solution densities, which also vary with RH, are needed. Two
665 important outputs of common aerosol thermodynamic models, such as E-AIM (Clegg et al., 1998)
666 and ISORROPIA II (Fountoukis and Nenes, 2007) are volumes and water-to-solute ratios as a
667 function of RH (above DRH) for aqueous solutions. Water-to-solute ratios and particle diameters
668 were both measured in our work at different RH, and our experimental data, when compared with
669 theoretical calculations, can be used to validate these thermodynamic models.

670 When RH are lower than the DRH of $\text{Ca}(\text{NO}_3)_2 \cdot 4\text{H}_2\text{O}$, aerosol particles used in our H-
671 TDMA experiments, instead of bulk samples used in the VSA measurements, are of direct
672 atmospheric relevance, and hence the H-TDMA results should be used in atmospheric **applications**.
673 There are still some open questions regarding $\text{Ca}(\text{NO}_3)_2$ aerosol particles (as well as other types of
674 particles investigated in this work) for RH below DRH of $\text{Ca}(\text{NO}_3)_2 \cdot 4\text{H}_2\text{O}$. What is the phase state

675 of aerosol particles at different RH? Are they crystalline solid, amorphous solid (glassy), or
676 supersaturated solutions? In this aspect, measurements of particle phase state of $\text{Ca}(\text{NO}_3)_2$ and
677 other aerosols considered in our work, using the apparatus described previously (Li et al., 2017),
678 can shed some light. Furthermore, how do water-to-solute ratios change with RH for $\text{Ca}(\text{NO}_3)_2$
679 aerosol particles when RH is below the DRH of $\text{Ca}(\text{NO}_3)_2 \cdot 4\text{H}_2\text{O}$? This can be answered by
680 determining particle mass as a function of RH for aerosol particles, and techniques are now
681 available for this task (Vlasenko et al., 2017).

682 **3.3.2 Atmospheric implications**

683 Hygroscopicity of carbonate minerals, such as calcite and dolomite, is initially very low
684 and can be largely enhanced due to formation of more hygroscopic materials via heterogeneous
685 reactions during transport (Tang et al., 2016a). Our present work investigated the hygroscopic
686 properties of eight Ca- or Mg-containing compounds which are aging products formed via
687 heterogeneous reactions of carbonate minerals, and revealed that the hygroscopicity of these
688 products is significantly higher than original carbonate minerals. In addition, hygroscopicity was
689 found to differ for different aging products, suggesting that heterogeneous reactions with different
690 trace gases may have distinctive effects on the hygroscopicity of carbonate minerals. For example,
691 the hygroscopicity of $\text{Ca}(\text{NO}_3)_2$ and CaCl_2 , formed through heterogeneous reactions with nitrogen
692 oxides and HCl, is much higher than that for $\text{Ca}(\text{HCOO})_2$ and $\text{Ca}(\text{CH}_3\text{COO})_2$, formed via
693 heterogeneous reactions with formic and acetic acids. Our work also observed that significant
694 hygroscopic growth of aerosol particles, such as $\text{Ca}(\text{NO}_3)_2$ and CaCl_2 , occurred at RH as low as
695 10%. This implies that aged carbonate particles can take up significant amount of water even under
696 very low RH, leading to changes in their diameters and morphology and thus impacting their
697 optical properties and direct radiative effects (Pan et al., 2015; Pan et al., 2018).

698 Large amounts of saline mineral dust are emitted into the atmosphere from dry lake beds
699 (Prospero et al., 2002), but these particles are usually assumed to be nonhygroscopic. Gaston et al.
700 (2017) found that saline mineral dust particles from different sources exhibit very different CCN
701 activities, and the measured κ_{ccn} varied from <0.01 to >0.8 , depending on the abundance of soluble
702 components (e.g., chlorides and sulfates) contained in these particles. Saline mineral dust particles
703 **from different sources** are very likely to have different hygroscopic properties under subsaturation.
704 To understand the hygroscopic growth of saline mineral dust particles, knowledge in hygroscopic
705 growth as well as the abundance of soluble components they contain is needed. Since CaCl_2 and
706 MgCl_2 have been identified as important components in saline mineral dust, their hygroscopicity
707 data measured in our work will be useful for improving our knowledge in hygroscopic properties
708 of saline mineral dust.

709 It is conventionally assumed that the hygroscopicity of sea salt is very similar to that of
710 pure NaCl. However, a recent study (Zieger et al., 2017) suggested that the hygroscopic growth
711 factor of sea salt aerosol at 90% RH is 8-15% lower than NaCl aerosol, and this difference is
712 attributed to the presence of MgCl_2 and CaCl_2 hydrates in sea salt. Growth factors at 90% RH were
713 measured in our work to be ~ 1.7 for MgCl_2 and CaCl_2 aerosols, significant lower than for NaCl
714 (2.29-2.46) (Zieger et al., 2017). Therefore, our work provides further experimental results to
715 support the conclusion drawn by Zieger et al. (2017), and would help better understand the
716 hygroscopicity of sea salt aerosol.

717 **4. Summary and Conclusion**

718 Ca- and Mg-containing salts, including nitrates, chlorides, formates and acetates, are
719 important components for mineral dust and sea salt aerosols; however, their hygroscopic properties
720 are not well understood yet. In this work, phase transition and hygroscopic growth of eight Ca- or

721 Mg-containing compounds were systematically examined using a vapor sorption analyzer and a
722 humidity-tandem differential mobility analyzer. DRH values decreased from $60.5\pm 1.0\%$ at $5\text{ }^{\circ}\text{C}$ to
723 $46.0\pm 1.0\%$ at $30\text{ }^{\circ}\text{C}$ for $\text{Ca}(\text{NO}_3)_2\cdot 4\text{H}_2\text{O}$ and from $57.5\pm 1.0\%$ at $5\text{ }^{\circ}\text{C}$ to $50.5\pm 1.0\%$ at $30\text{ }^{\circ}\text{C}$ for
724 $\text{Mg}(\text{NO}_3)_2\cdot 6\text{H}_2\text{O}$, both showing negative dependence on temperature, and this dependence can be
725 approximated by the Clausius-Clapeyron equation. No significant dependence of DRH (around
726 31-33%) on temperature ($5\text{-}30\text{ }^{\circ}\text{C}$) was observed for $\text{MgCl}_2\cdot 6\text{H}_2\text{O}$. $\text{CaCl}_2\cdot 6\text{H}_2\text{O}$, found to
727 deliquesce at $\sim 28.5\%$ RH at $25\text{ }^{\circ}\text{C}$, exhibited complex phase transition processes in which
728 $\text{CaCl}_2\cdot 2\text{H}_2\text{O}$, $\text{CaCl}_2\cdot 6\text{H}_2\text{O}$ and aqueous CaCl_2 solutions were involved. Furthermore, DRH values
729 were determined to be $90.5\pm 1.0\%$ for $\text{Ca}(\text{CH}_3\text{COO})_2\cdot \text{H}_2\text{O}$ and $71.5\pm 1.0\%$ for
730 $\text{Mg}(\text{CH}_3\text{COO})_2\cdot 4\text{H}_2\text{O}$ at $25\text{ }^{\circ}\text{C}$; for comparison, the sample mass was only increased by $\sim 12\%$ for
731 $\text{Ca}(\text{HCOO})_2$ and $\sim 6\%$ for $\text{Mg}(\text{HCOO})_2\cdot 2\text{H}_2\text{O}$ when RH was increased from 0 to 95%, implying
732 that the DRH of these two compounds were probably $>95\%$.

733 We have also measured the change of sample mass as a function of RH up to 90% to derive
734 the water-to-solute ratios (WSR) for deliquesced samples. WSR were determined at 25 and $5\text{ }^{\circ}\text{C}$
735 for deliquesced $\text{Ca}(\text{NO}_3)_2\cdot 4\text{H}_2\text{O}$, $\text{Mg}(\text{NO}_3)_2\cdot 6\text{H}_2\text{O}$ and $\text{MgCl}_2\cdot 6\text{H}_2\text{O}$ samples, and at $25\text{ }^{\circ}\text{C}$ for
736 deliquesced $\text{CaCl}_2\cdot 6\text{H}_2\text{O}$ and $\text{Mg}(\text{CH}_3\text{COO})_2\cdot 4\text{H}_2\text{O}$ samples. We found that compared to that at 0%
737 RH, large increases in sample mass only occurred when RH was increased from 90 to 95% for
738 $\text{Ca}(\text{CH}_3\text{COO})_2\cdot \text{H}_2\text{O}$, and the WSR value was determined to be 5.849 ± 0.064 at 95% RH. Besides,
739 deliquescence was not observed even when RH was increased to 95% for $\text{Ca}(\text{HCOO})_2$ and
740 $\text{Mg}(\text{HCOO})_2\cdot 2\text{H}_2\text{O}$, and the ratios of sample mass at 95% to that at 0% RH, were determined to
741 be for 1.119 ± 0.036 for $\text{Ca}(\text{HCOO})_2$ and 1.064 ± 0.020 for $\text{Mg}(\text{HCOO})_2\cdot 2\text{H}_2\text{O}$. Despite that
742 compounds investigated in the present work are important components for tropospheric aerosols,
743 in general they have not been included in widely used aerosol thermodynamic models, such as E-

744 AIM (Clegg et al., 1998) and ISORROPIA II (Fountoukis and Nenes, 2007). The systematical and
745 comprehensive datasets which we have obtained in this work are highly valuable and can be used
746 to validate thermodynamic models if they are extended to include these compounds.

747 In addition, hygroscopic growth of aerosol particles was measured at room temperature for
748 these eight compounds. Being different from solid samples for which the onset of deliquescence
749 was evident, aerosol particles were found to grow in a continuous manner since very low RH (as
750 low as 10%), implying that **these** dry aerosol particles generated from aqueous droplets were
751 amorphous. Hygroscopic growth factors of aerosol particles at 90% RH were determined to be
752 1.79 ± 0.03 and 1.67 ± 0.03 for $\text{Ca}(\text{NO}_3)_2$ and $\text{Mg}(\text{NO}_3)_2$, 1.71 ± 0.03 for both CaCl_2 and MgCl_2 ,
753 1.54 ± 0.02 and 1.69 ± 0.03 for $\text{Ca}(\text{HCOO})_2$ and $\text{Mg}(\text{HCOO})_2$, and 1.26 ± 0.04 and 1.53 ± 0.01 for
754 $\text{Ca}(\text{HCOO})_2$ and $\text{Mg}(\text{HCOO})_2$. GF at 90% show significant variation (from ~ 1.26 to ~ 1.79) for the
755 Ca-containing salts investigated here; among them nitrate and chloride have very similar GF
756 (1.79 ± 0.03 versus 1.71 ± 0.03), which are larger than that of formate (1.54 ± 0.02), while acetate has
757 the smallest GF (1.26 ± 0.04). Interestingly, for the four Mg-containing salts considered in this work,
758 the variation in GF at 90 % RH was found to be much smaller (from ~ 1.53 to ~ 1.71).

759 GF at 90% RH were used to derive the single hygroscopicity parameters (κ), which were
760 determined to be 0.49-0.56 and 0.38-0.43 for $\text{Ca}(\text{NO}_3)_2$ and $\text{Mg}(\text{NO}_3)_2$, 0.42-0.47 for both CaCl_2
761 and MgCl_2 , 0.28-0.31 and 0.40-0.45 for $\text{Ca}(\text{HCOO})_2$ and $\text{Mg}(\text{HCOO})_2$, and 0.09-0.13 and 0.28-
762 0.29 for $\text{Ca}(\text{HCOO})_2$ and $\text{Mg}(\text{HCOO})_2$ aerosols, respectively. $\text{Ca}(\text{NO}_3)_2$ and CaCl_2 are very soluble
763 in water, and thus their κ values derived from our H-TDMA experiments are consistent with those
764 reported by previous CCN activity measurements (Sullivan et al., 2009; Tang et al., 2015); on the
765 other hand, due to limited water solubilities, for $\text{Ca}(\text{HCOO})_2$ and $\text{Ca}(\text{CH}_3\text{COO})_2$, κ values derived
766 from our H-TDMA experiments are significantly smaller than those derived from CCN activities

767 (Tang et al., 2015). Overall, the present work would significantly improve our knowledge in the
768 hygroscopic properties of Ca- and Mg-containing salts, and thereby help better understand the
769 physicochemical properties of mineral dust and sea salt aerosols.

770 **Author contribution**

771 Mingjin Tang designed the research; Liya Guo, Peng Chao, Taomou Zong, Qinhao Lin and
772 Guohua Zhang did the H-TDMA experiments and analyzed the results with the assistance and
773 supervision of Weigang Wang, Zhijun Wu, Maofa Ge, Min Hu and Xinhui Bi; Wenjun Gu and
774 Yujing Tang did the VSA experiments and analyzed the data with the supervision of Yong Jie Li,
775 Xinming Wang and Mingjin Tang; Yong Jie Li and Mingjin Tang wrote the manuscript with the
776 contribution from all the other co-authors.

777 **Acknowledgement**

778 This work was funded by the National Natural Science Foundation of China (91744204,
779 91644106 and 41675120), the Chinese Academy of Sciences international collaborative project
780 (132744KYSB20160036) and the special fund of State Key Joint Laboratory of Environment
781 Simulation and Pollution Control (17K02ESPCP). Mingjin Tang also would like to thank the CAS
782 Pioneer Hundred Talents program for providing a starting grant. Yujing Tang contributed to this
783 work as an undergraduate intern at Guangzhou Institute of Geochemistry. This is contribution No.
784 IS-XXX from GIGCAS.

785 **References**

786 Adams, J. R., and Merz, A. R.: Hygroscopicity of Fertilizer Materials and Mixtures, *Ind. Eng. Chem.*, 21, 305-307,
787 1929.
788 Al-Abadleh, H. A., and Grassian, V. H.: Phase transitions in magnesium nitrate thin films: A transmission FT-IR
789 study of the deliquescence and efflorescence of nitric acid reacted magnesium oxide interfaces, *J. Phys. Chem. B*,
790 107, 10829-10839, 2003.
791 Al-Abadleh, H. A., Krueger, B. J., Ross, J. L., and Grassian, V. H.: Phase transitions in calcium nitrate thin films,
792 *Chem. Commun.*, 2796-2797, 2003.

793 Apelblat, A.: The vapor pressures of water over saturated solutions of barium chloride, magnesium nitrate, calcium
794 nitrate, potassium carbonate, and zinc sulfate at temperatures from 283 K to 323 K, *J. Chem. Thermodyn.*, 24, 619-
795 626, 1992.

796 Biggs, A. I., Parton, H. N., and Robinson, R. A.: The Constitution of the Lead Halides in Aqueous Solution, *J. Am.*
797 *Chem. Soc.*, 77, 5844-5848, 1955.

798 Chang, R. Y. W., Liu, P. S. K., Leaitch, W. R., and Abbatt, J. P. D.: Comparison between measured and predicted
799 CCN concentrations at Egbert, Ontario: Focus on the organic aerosol fraction at a semi-rural site, *Atmos. Environ.*,
800 41, 8172-8182, 2007.

801 Chen, S. Y., Huang, J. P., Kang, L. T., Wang, H., Ma, X. J., He, Y. L., Yuan, T. G., Yang, B., Huang, Z. W., and
802 Zhang, G. L.: Emission, transport, and radiative effects of mineral dust from the Taklimakan and Gobi deserts:
803 comparison of measurements and model results, *Atmos. Chem. Phys.*, 17, 2401-2421, 2017.

804 Clegg, S. L., Brimblecombe, P., and Wexler, A. S.: Thermodynamic Model of the System $H^+-NH_4^+-Na^+-SO_4^{2-}$
805 $-NO_3^- -Cl^- -H_2O$ at 298.15 K, *J. Phys. Chem. A.*, 102, 2155-2171, 1998.

806 Creamean, J. M., Suski, K. J., Rosenfeld, D., Cazorla, A., DeMott, P. J., Sullivan, R. C., White, A. B., Ralph, F. M.,
807 Minnis, P., Comstock, J. M., Tomlinson, J. M., and Prather, K. A.: Dust and Biological Aerosols from the Sahara
808 and Asia Influence Precipitation in the Western U.S, *Science*, 339, 1572-1578, 2013.

809 Crowley, J. N., Ammann, M., Cox, R. A., Hynes, R. G., Jenkin, M. E., Mellouki, A., Rossi, M. J., Troe, J., and
810 Wallington, T. J.: Evaluated Kinetic and Photochemical Data for Atmospheric Chemistry: Volume V -
811 Heterogeneous Reactions on Solid Substrates, *Atmos. Chem. Phys.*, 10, 9059-9223, 2010.

812 Cziczco, D. J., and Abbatt, J. P. D.: Infrared observations of the response of NaCl, MgCl₂, NH₄HSO₄, and NH₄NO₃
813 aerosols to changes in relative humidity from 298 to 238 K, *J. Phys. Chem. A*, 104, 2038-2047, 2000.

814 Cziczco, D. J., Froyd, K. D., Hoose, C., Jensen, E. J., Diao, M., Zondlo, M. A., Smith, J. B., Twohy, C. H., and
815 Murphy, D. M.: Clarifying the Dominant Sources and Mechanisms of Cirrus Cloud Formation, *Science*, 340, 1320-
816 1324, 2013.

817 Dean, J. A.: *Lange's Handbook on Chemistry (Eleventh Edition)*, McGraw-Hill, Inc., New York, 1973.

818 El Guendouzi, M., and Marouani, M.: Water activities and osmotic and activity coefficients of aqueous solutions of
819 nitrates at 25 degrees C by the hygrometric method, *J. Solution Chem.*, 32, 535-546, 2003.

820 Formenti, P., Rajot, J. L., Desboeufs, K., Saïd, F., Grand, N., Chevaillier, S., and Schmechtig, C.: Airborne
821 observations of mineral dust over western Africa in the summer Monsoon season: spatial and vertical variability of
822 physico-chemical and optical properties, *Atmos. Chem. Phys.*, 11, 6387-6410, 2011.

823 Formenti, P., Caquineau, S., Desboeufs, K., Klaver, A., Chevaillier, S., Journet, E., and Rajot, J. L.: Mapping the
824 physico-chemical properties of mineral dust in western Africa: mineralogical composition, *Atmos. Chem. Phys.*, 14,
825 10663-10686, 2014.

826 Fountoukis, C., and Nenes, A.: ISORROPIA II: a computationally efficient thermodynamic equilibrium model for
827 $K^+-Ca^{2+}-Mg^{2+}-NH_4^+-Na^+-SO_4^{2-}-NO_3^- -Cl^- -H_2O$ aerosols, *Atmos. Chem. Phys.*, 7, 4639-4659, 2007.

828 Gaston, C. J., Pratt, K. A., Suski, K. J., May, N. W., Gill, T. E., and Prather, K. A.: Laboratory Studies of the Cloud
829 Droplet Activation Properties and Corresponding Chemistry of Saline Playa Dust, *Environ. Sci. Technol.*, 51, 1348-
830 1356, 2017.

831 Gibson, E. R., Hudson, P. K., and Grassian, V. H.: Physicochemical properties of nitrate aerosols: Implications for
832 the atmosphere, *J. Phys. Chem. A*, 110, 11785-11799, 2006.

833 Ginoux, P., Prospero, J. M., Gill, T. E., Hsu, N. C., and Zhao, M.: Global-scale Attribution of Anthropogenic and
834 Natural Dust Sources and Their Emission Rates Based on MODIS Deep Blue Aerosol Products, *Rev. Geophys.*, 50,
835 RG3005, doi: 3010.1029/2012RG000388, 2012.

836 Good, N., Topping, D. O., Duplissy, J., Gysel, M., Meyer, N. K., Metzger, A., Turner, S. F., Baltensperger, U.,
837 Ristovski, Z., Weingartner, E., Coe, H., and McFiggans, G.: Widening the gap between measurement and modelling
838 of secondary organic aerosol properties?, *Atmos. Chem. Phys.*, 10, 2577-2593, 2010.

839 Goodman, A. L., Underwood, G. M., and Grassian, V. H.: A Laboratory Study of the Heterogeneous Reaction of
840 Nitric Acid on Calcium Carbonate Particles, *J. Geophys. Res.-Atmos.*, 105, 29053-29064, 2000.

841 Gough, R. V., Chevrier, V. F., and Tolbert, M. A.: Formation of liquid water at low temperatures via the
842 deliquescence of calcium chloride: Implications for Antarctica and Mars, *Planet. Space Sci.*, 131, 79-87, 2016.

843 Gu, W. J., Li, Y. J., Tang, M. J., Jia, X. H., Ding, X., Bi, X. H., and Wang, X. M.: Water uptake and hygroscopicity
844 of perchlorates and implications for the existence of liquid water in some hyperarid environments, *RSC Adv.*, 7,
845 46866-46873, 2017a.

846 Gu, W. J., Li, Y. J., Zhu, J. X., Jia, X. H., Lin, Q. H., Zhang, G. H., Ding, X., Song, W., Bi, X. H., Wang, X. M., and
847 Tang, M. J.: Investigation of water adsorption and hygroscopicity of atmospherically relevant particles using
848 a commercial vapor sorption analyzer, *Atmos. Meas. Tech.*, 10, 3821-3832, 2017b.

849 Gupta, D., Eom, H. J., Cho, H. R., and Ro, C. U.: Hygroscopic behavior of NaCl-MgCl₂ mixture particles as nascent
850 sea-spray aerosol surrogates and observation of efflorescence during humidification, *Atmos. Chem. Phys.*, 15,
851 11273-11290, 2015.

852 Gysel, M., McFiggans, G. B., and Coe, H.: Inversion of tandem differential mobility analyser (TDMA)
853 measurements, *J. Aerosol. Sci.*, 40, 134-151, 2009.

854 Ha, Z., and Chan, C. K.: The Water Activities of MgCl₂, Mg(NO₃)₂, MgSO₄, and Their Mixtures, *Aerosol Sci.*
855 *Technol.*, 31, 154-169, 1999.

856 Hatch, C. D., Gough, R. V., and Tolbert, M. A.: Heterogeneous Uptake of the C1 to C4 Organic Acids on a Swelling
857 Clay Mineral, *Atmos. Chem. Phys.*, 7, 4445-4458, 2007.

858 Hoose, C., and Moehler, O.: Heterogeneous ice nucleation on atmospheric aerosols: a review of results from
859 laboratory experiments, *Atmos. Chem. Phys.*, 12, 9817-9854, 2012.

860 Jeong, G. Y., and Achterberg, E. P.: Chemistry and mineralogy of clay minerals in Asian and Saharan dusts and the
861 implications for iron supply to the oceans, *Atmos. Chem. Phys.*, 14, 12415-12428, 2014.

862 Jia, X. H., Gu, W. J., Li, Y. J., Cheng, P., Tang, Y. J., Guo, L. Y., Wang, X. M., and Tang, M. J.: Phase transitions
863 and hygroscopic growth of Mg(ClO₄)₂, NaClO₄, and NaClO₄·H₂O: implications for the stability of aqueous water
864 in hyperarid environments on Mars and on Earth, *ACS Earth Space Chem.*, 2, 159-167, 2018.

865 Jickells, T. D., An, Z. S., Andersen, K. K., Baker, A. R., Bergametti, G., Brooks, N., Cao, J. J., Boyd, P. W., Duce,
866 R. A., Hunter, K. A., Kawahata, H., Kubilay, N., laRoche, J., Liss, P. S., Mahowald, N., Prospero, J. M., Ridgwell,
867 A. J., Tegen, I., and Torres, R.: Global Iron Connections between Desert Dust, Ocean Biogeochemistry, and
868 Climate, *Science*, 308, 67-71, 2005.

869 Jing, B., Tong, S. R., Liu, Q. F., Li, K., Wang, W. G., Zhang, Y. H., and Ge, M. F.: Hygroscopic behavior of
870 multicomponent organic aerosols and their internal mixtures with ammonium sulfate, *Atmos. Chem. Phys.*, 16,
871 4101-4118, 2016.

872 Jing, B., Wang, Z., Tan, F., Guo, Y. C., Tong, S. R., Wang, W. G., Zhang, Y. H., and Ge, M. F.: Hygroscopic
873 behavior of atmospheric aerosols containing nitrate salts and water-soluble organic acids, *Atmos. Chem. Phys.*, 18,
874 5115-5127, 2018.

875 Journet, E., Balkanski, Y., and Harrison, S. P.: A New Data Set of Soil Mineralogy for Dust-cycle Modeling, *Atmos.*
876 *Chem. Phys.*, 14, 3801-3816, 2014.

877 Kelly, J. T., and Wexler, A. S.: Thermodynamics of carbonates and hydrates related to heterogeneous reactions
878 involving mineral aerosol, *J. Geophys. Res.-Atmos.*, 110, D11201, doi: 11210.11029/12004jd005583, 2005.

879 Kelly, J. T., Chuang, C. C., and Wexler, A. S.: Influence of dust composition on cloud droplet formation, *Atmos.*
880 *Environ.*, 41, 2904-2916, 2007.

881 Khare, P., Kumar, N., Kumari, K. M., and Srivastava, S. S.: Atmospheric formic and acetic acids: An overview,
882 *Rev. Geophys.*, 37, 227-248, 1999.

883 Koehler, K. A., Kreidenweis, S. M., DeMott, P. J., Petters, M. D., Prenni, A. J., and Carrico, C. M.: Hygroscopicity
884 and cloud droplet activation of mineral dust aerosol, *Geophys. Res. Lett.*, 36, L08805, doi:
885 08810.01029/02009gl037348, 2009.

886 Kreidenweis, S. M., and Asa-Awuku, A.: 5.13 - Aerosol Hygroscopicity: Particle Water Content and Its Role in
887 Atmospheric Processes, in: *Treatise on Geochemistry (Second Edition)*, edited by: Turekian, K. K., Elsevier,
888 Oxford, 331-361, 2014.

889 Krueger, B. J., Grassian, V. H., Laskin, A., and Cowin, J. P.: The Transformation of Solid Atmospheric Particles
890 into Liquid Droplets through Heterogeneous Chemistry: Laboratory Insights into the Processing of Calcium
891 Containing Mineral Dust Aerosol in the Troposphere, *Geophys. Res. Lett.*, 30, 1148, doi: 1110.1029/2002gl016563,
892 2003.

893 Laskin, A., Iedema, M. J., Ichkovich, A., Graber, E. R., Taraniuk, I., and Rudich, Y.: Direct Observation of
894 Completely Processed Calcium Carbonate Dust Particles, *Faraday Discuss.*, 130, 453-468, 2005.

895 Lei, T., Zuend, A., Wang, W. G., Zhang, Y. H., and Ge, M. F.: Hygroscopicity of organic compounds from biomass
896 burning and their influence on the water uptake of mixed organic ammonium sulfate aerosols, *Atmos. Chem. Phys.*,
897 14, 11165-11183, 2014.

898 Li, H. J., Zhu, T., Zhao, D. F., Zhang, Z. F., and Chen, Z. M.: Kinetics and mechanisms of heterogeneous reaction of
899 NO₂ on CaCO₃ surfaces under dry and wet conditions, *Atmos. Chem. Phys.*, 10, 463-474, 2010.

900 Li, W. J., and Shao, L. Y.: Observation of Nitrate Coatings on Atmospheric Mineral Dust Particles, *Atmos. Chem.*
901 *Phys.*, 9, 1863-1871, 2009.

902 Li, X.-H., Zhao, L.-J., Dong, J.-L., Xiao, H.-S., and Zhang, Y.-H.: Confocal Raman Studies of Mg(NO₃)₂ Aerosol
903 Particles Deposited on a Quartz Substrate: Supersaturated Structures and Complicated Phase Transitions, *J. Phys.*
904 *Chem. B.*, 112, 5032-5038, 2008a.

905 Li, X., Dong, J., Xiao, H., Lu, P., Hu, Y., and Zhang, Y.: FTIR-ATR in situ observation on the efflorescence and
906 deliquescence processes of $Mg(NO_3)_2$ aerosols, *Sci. China-Chem.*, 51, 128-137, 2008b.

907 Li, Y. J., Liu, P. F., Bergoend, C., Bateman, A. P., and Martin, S. T.: Rebounding hygroscopic inorganic aerosol
908 particles: Liquids, gels, and hydrates, *Aerosol Sci. Technol.*, 51, 388-396, 2017.

909 Liu, Y., Gibson, E. R., Cain, J. P., Wang, H., Grassian, V. H., and Laskin, A.: Kinetics of heterogeneous reaction of
910 $CaCO_3$ particles with gaseous HNO_3 over a wide range of humidity, *J. Phys. Chem. A*, 112, 1561-1571, 2008a.

911 Liu, Y. J., Zhu, T., Zhao, D. F., and Zhang, Z. F.: Investigation of the hygroscopic properties of $Ca(NO_3)_2$ and
912 internally mixed $Ca(NO_3)_2/CaCO_3$ particles by micro-Raman spectrometry, *Atmos. Chem. Phys.*, 8, 7205-7215,
913 2008b.

914 Ma, Q. X., Liu, Y. C., Liu, C., and He, H.: Heterogeneous Reaction of Acetic Acid on MgO , $\alpha-Al_2O_3$, and $CaCO_3$
915 and the Effect on the Hygroscopic Behavior of These Particles, *Phys. Chem. Chem. Phys.*, 14, 8403-8409, 2012.

916 Mahowald, N., Ward, D. S., Kloster, S., Flanner, M. G., Heald, C. L., Heavens, N. G., Hess, P. G., Lamarque, J.-F.,
917 and Chuang, P. Y.: Aerosol Impacts on Climate and Biogeochemistry, *Annu. Rev. Environ. Resour.*, 36, 45-74,
918 2011.

919 Mahowald, N. M., Engelstaedter, S., Luo, C., Sealy, A., Artaxo, P., Benitez-Nelson, C., Bonnet, S., Chen, Y.,
920 Chuang, P. Y., Cohen, D. D., Dulac, F., Herut, B., Johansen, A. M., Kubilay, N., Losno, R., Maenhaut, W., Paytan,
921 A., Prospero, J. M., Shank, L. M., and Siefert, R. L.: Atmospheric Iron Deposition: Global Distribution, Variability,
922 and Human Perturbations, *Ann. Rev. Mar. Sci.*, 1, 245-278, 2009.

923 Massoli, P., Lambe, A. T., Ahern, A. T., Williams, L. R., Ehn, M., Mikkila, J., Canagaratna, M. R., Brune, W. H.,
924 Onasch, T. B., Jayne, J. T., Petaja, T., Kulmala, M., Laaksonen, A., Kolb, C. E., Davidovits, P., and Worsnop, D. R.:
925 Relationship between aerosol oxidation level and hygroscopic properties of laboratory generated secondary organic
926 aerosol (SOA) particles, *Geophys. Res. Lett.*, 37, L24801, DOI: 24810.21029/22010GL045258, 2010.

927 Nickovic, S., Vukovic, A., Vujadinovic, M., Djurdjevic, V., and Pejanovic, G.: Technical Note: High-resolution
928 mineralogical database of dust-productive soils for atmospheric dust modeling, *Atmos. Chem. Phys.*, 12, 845-855,
929 2012.

930 Pan, X., Uno, I., Hara, Y., Kuribayashi, M., Kobayashi, H., Sugimoto, N., Yamamoto, S., Shimohara, T., and Wang,
931 Z.: Observation of the simultaneous transport of Asian mineral dust aerosols with anthropogenic pollutants using a
932 POPC during a long-lasting dust event in late spring 2014, *Geophys. Res. Lett.*, 42, 1593-1598, 2015.

933 Pan, X., Uno, I., Wang, Z., Nishizawa, T., Sugimoto, N., Yamamoto, S., Kobayashi, H., Sun, Y., Fu, P., Tang, X.,
934 and Wang, Z.: Real-time observational evidence of changing Asian dust morphology with the mixing of heavy
935 anthropogenic pollution, *Sci. Rep.*, 7, 335, doi: 310.1038/s41598-41017-00444-w, 2017.

936 Pan, X., Ge, B., Wang, Z., Tian, Y., Liu, H., Wei, L., Yue, S., Uno, I., Kobayashi, H., Nishizawa, T., Shimizu, A.,
937 Fu, P., and Wang, Z.: Synergistic effect of water-soluble species and relative humidity on morphological changes of
938 aerosol particles in Beijing mega-city during severe pollution episodes, *Atmos. Chem. Phys. Discuss.*, 2018, 1-24,
939 10.5194/acp-2018-623, 2018.

940 Pang, S. F., Wu, C. Q., Zhang, Q. N., and Zhang, Y. H.: The structural evolution of magnesium acetate complex in
941 aerosols by FTIR-ATR spectra, *J. Mol. Struct.*, 1087, 46-50, 2015.

942 Park, K., Kim, J. S., and Miller, A. L.: A study on effects of size and structure on hygroscopicity of nanoparticles
943 using a tandem differential mobility analyzer and TEM, *J. Nanopart. Res.*, 11, 175-183, 2009.

944 Peng, C., Jing, B., Guo, Y. C., Zhang, Y. H., and Ge, M. F.: Hygroscopic Behavior of Multicomponent Aerosols
945 Involving NaCl and Dicarboxylic Acids, *J. Phys. Chem. A*, 120, 1029-1038, 2016.

946 Petters, M. D., and Kreidenweis, S. M.: A single parameter representation of hygroscopic growth and cloud
947 condensation nucleus activity, *Atmos. Chem. Phys.*, 7, 1961-1971, 2007.

948 Petters, M. D., and Kreidenweis, S. M.: A single parameter representation of hygroscopic growth and cloud
949 condensation nucleus activity-Part 2: Including solubility, *Atmos. Chem. Phys.*, 8, 6273-6279, 2008.

950 Petters, M. D., Wex, H., Carrico, C. M., Hallbauer, E., Massling, A., McMeeking, G. R., Poulain, L., Wu, Z.,
951 Kreidenweis, S. M., and Stratmann, F.: Towards closing the gap between hygroscopic growth and activation for
952 secondary organic aerosol - Part 2: Theoretical approaches, *Atmos. Chem. Phys.*, 9, 3999-4009, 2009.

953 Prenni, A. J., Petters, M. D., Kreidenweis, S. M., DeMott, P. J., and Ziemann, P. J.: Cloud droplet activation of
954 secondary organic aerosol, *J. Geophys. Res.-Atmos.*, 112, D10223, DOI: 10210.11029/12006JD007963, 2007.

955 Prince, A. P., Kleiber, P. D., Grassian, V. H., and Young, M. A.: Reactive Uptake of Acetic Acid on Calcite and
956 Nitric Acid Reacted Calcite Aerosol in an Environmental Reaction Chamber, *Phys. Chem. Chem. Phys.*, 10, 142-
957 152, 2008.

958 Prospero, J. M., Ginoux, P., Torres, O., Nicholson, S. E., and Gill, T. E.: Environmental characterization of global
959 sources of atmospheric soil dust identified with the Nimbus 7 Total Ozone Mapping Spectrometer (TOMS)
960 absorbing aerosol product, *Rev. Geophys.*, 40, 1002, DOI: 1010.1029/2000RG000095, 2002.

961 Rard, J. A., Habenschuss, A., and Spedding, F. H.: A review of the osmotic coefficients of aqueous calcium chloride
962 at 25 °C, *J. Chem. Eng. Data*, 22, 180-186, 1977.

963 Rard, J. A., and Miller, D. G.: Isopiestic determination of the osmotic and activity coefficients of aqueous
964 magnesium chloride solutions at 25 °C, *J. Chem. Eng. Data*, 26, 38-43, 1981.

965 Rard, J. A., Wijesinghe, A. M., and Wolery, T. J.: Review of the thermodynamic properties of Mg(NO₃)₂(aq) and
966 their representation with the standard and extended ion-interaction (Pitzer) models at 298.15 K, *J. Chem. Eng. Data*,
967 49, 1127-1140, 2004.

968 Ridley, D. A., Heald, C. L., Kok, J. F., and Zhao, C.: An observationally constrained estimate of global dust aerosol
969 optical depth, *Atmos. Chem. Phys.*, 16, 15097-15117, 2016.

970 Robinson, R. A., and Stokes, R. H.: *Electrolyte Solutions (Second Revised Edition)*, Butterworths, London, UK,
971 1959.

972 Romanias, M. N., El Zein, A., and Bedjanian, Y.: Heterogeneous Interaction of H₂O₂ with TiO₂ Surface under Dark
973 and UV Light Irradiation Conditions, *J. Phys. Chem. A*, 116, 8191-8200, 2012.

974 Romanias, M. N., Zeineddine, M. N., Gaudion, V., Lun, X., Thevenet, F., and Riffault, V.: Heterogeneous
975 Interaction of Isopropanol with Natural Gobi Dust, *Environ. Sci. Technol.*, 50, 11714-11722, 2016.

976 Santschi, C., and Rossi, M. J.: Uptake of CO₂, SO₂, HNO₃ and HCl on calcite (CaCO₃) at 300 K: Mechanism and
977 the role of adsorbed water, *J. Phys. Chem. A*, 110, 6789-6802, 2006.

978 Scanza, R. A., Mahowald, N., Ghan, S., Zender, C. S., Kok, J. F., Liu, X., Zhang, Y., and Albani, S.: Modeling Dust
979 as Component Minerals in the Community Atmosphere Model: Development of Framework and Impact on
980 Radiative Forcing, *Atmos. Chem. Phys.*, 15, 537-561, 2015.

981 Seinfeld, J. H., and Pandis, S. N.: *Atmospheric Chemistry and Physics: From Air Pollution to Climate Change*
982 (Third edition), Wiley Interscience, New York, 2016.

983 Shi, Z., Zhang, D., Hayashi, M., Ogata, H., Ji, H., and Fujjie, W.: Influences of sulfate and nitrate on the
984 hygroscopic behaviour of coarse dust particles, *Atmos. Environ.*, 42, 822-827, 2008.

985 Sullivan, R. C., Moore, M. J. K., Petters, M. D., Kreidenweis, S. M., Roberts, G. C., and Prather, K. A.: Effect of
986 Chemical Mixing State on the Hygroscopicity and Cloud Nucleation Properties of Calcium Mineral Dust Particles,
987 *Atmos. Chem. Phys.*, 9, 3303-3316, 2009.

988 Tan, F., Tong, S. R., Jing, B., Hou, S., Liu, Q., Li, K., Zhang, Y., and Ge, M. F.: Heterogeneous reactions of NO₂
989 with CaCO₃-(NH₄)₂SO₄ mixtures at different relative humidities, *Atmos. Chem. Phys.*, 16, 8081-8093, 2016.

990 Tang, I. N., and Fung, K. H.: Hydration and Raman scattering studies of levitated microparticles: Ba(NO₃)₂,
991 Sr(NO₃)₂, and Ca(NO₃)₂, *J. Chem. Phys.*, 106, 1653-1660, 1997.

992 Tang, M. J., Thieser, J., Schuster, G., and Crowley, J. N.: Kinetics and Mechanism of the Heterogeneous Reaction of
993 N₂O₅ with Mineral Dust Particles, *Phys. Chem. Chem. Phys.*, 14, 8551-8561, 2012.

994 Tang, M. J., Whitehead, J., Davidson, N. M., Pope, F. D., Alfarra, M. R., McFiggans, G., and Kalberer, M.: Cloud
995 Condensation Nucleation Activities of Calcium Carbonate and its Atmospheric Ageing Products, *Phys. Chem.*
996 *Chem. Phys.*, 17, 32194-32203, 2015.

997 Tang, M. J., Cziczo, D. J., and Grassian, V. H.: Interactions of Water with Mineral Dust Aerosol: Water Adsorption,
998 Hygroscopicity, Cloud Condensation and Ice Nucleation, *Chem. Rev.*, 116, 4205-4259, 2016a.

999 Tang, M. J., Larish, W., Fang, Y., Gankanda, A., and Grassian, V. H.: Heterogeneous Reactions of Acetic Acid with
1000 Oxide Surfaces: Effects of Mineralogy and Relative Humidity, *J. Phys. Chem. A*, 120, 5609-5616, 2016b.

1001 Tang, M. J., Huang, X., Lu, K. D., Ge, M. F., Li, Y. J., Cheng, P., Zhu, T., Ding, A. J., Zhang, Y. H., Gligorovski,
1002 S., Song, W., Ding, X., Bi, X. H., and Wang, X. M.: Heterogeneous reactions of mineral dust aerosol: implications
1003 for tropospheric oxidation capacity, *Atmos. Chem. Phys.*, 17, 11727-11777, 2017.

1004 Textor, C., Schulz, M., Guibert, S., Kinne, S., Balkanski, Y., Bauer, S., Bernsten, T., Berglen, T., Boucher, O., Chin,
1005 M., Dentener, F., Diehl, T., Easter, R., Feichter, H., Fillmore, D., Ghan, S., Ginoux, P., Gong, S., Grini, A.,
1006 Hendricks, J., Horowitz, L., Huang, P., Isaksen, I., Iversen, I., Kloster, S., Koch, D., Kirkevåg, A., Kristjansson, J.
1007 E., Krol, M., Lauer, A., Lamarque, J. F., Liu, X., Montanaro, V., Myhre, G., Penner, J., Pitari, G., Reddy, S., Seland,
1008 Ø., Stier, P., Takemura, T., and Tie, X.: Analysis and Quantification of the Diversities of Aerosol Life Cycles within
1009 AeroCom, *Atmos. Chem. Phys.*, 6, 1777-1813, 2006.

1010 Tobo, Y., Zhang, D. Z., Nakata, N., Yamada, M., Ogata, H., Hara, K., and Iwasaka, Y.: Hygroscopic mineral dust
1011 particles as influenced by chlorine chemistry in the marine atmosphere, *Geophys. Res. Lett.*, 36, L05817, doi:
1012 05810.01029/02008gl036883, 2009.

1013 Tobo, Y., Zhang, D., Matsuki, A., and Iwasaka, Y.: Asian Dust Particles Converted into Aqueous Droplets under
1014 Remote Marine Atmospheric Conditions, *Proc. Natl. Acad. Sci. U. S. A.*, 107, 17905-17910, 2010.

1015 Tong, S. R., Wu, L. Y., Ge, M. F., Wang, W. G., and Pu, Z. F.: Heterogeneous Chemistry of Monocarboxylic Acids
1016 on α-Al₂O₃ at Different Relative Humidities, *Atmos. Chem. Phys.*, 10, 7561-7574, 2010.

1017 Uno, I., Eguchi, K., Yumimoto, K., Takemura, T., Shimizu, A., Uematsu, M., Liu, Z., Wang, Z., Hara, Y., and
1018 Sugimoto, N.: Asian Dust Transported One Full Circuit around the Globe, *Nature Geosci.*, 2, 557-560, 2009.
1019 Usher, C. R., Michel, A. E., and Grassian, V. H.: Reactions on Mineral Dust, *Chem. Rev.*, 103, 4883-4939, 2003.
1020 Vlasenko, A., Sjogren, S., Weingartner, E., Gaggeler, H. W., and Ammann, M.: Generation of submicron Arizona
1021 test dust aerosol: Chemical and hygroscopic properties, *Aerosol Sci. Technol.*, 39, 452-460, 2005.
1022 Vlasenko, A., Sjogren, S., Weingartner, E., Stemmler, K., Gaggeler, H. W., and Ammann, M.: Effect of Humidity
1023 on Nitric Acid Uptake to Mineral Dust Aerosol Particles, *Atmos. Chem. Phys.*, 6, 2147-2160, 2006.
1024 Vlasenko, S. S., Su, H., Pöschl, U., Andreae, M. O., and Mikhailov, E. F.: Tandem configuration of differential
1025 mobility and centrifugal particle mass analysers for investigating aerosol hygroscopic properties, *Atmos. Meas.*
1026 *Tech.*, 10, 1269-1280, 2017.
1027 Wang, L. Y., Zhang, Y. H., and Zhao, L. J.: Raman spectroscopic studies on single supersaturated droplets of
1028 sodium and magnesium acetate, *J. Phys. Chem. A*, 109, 609-614, 2005.
1029 Wex, H., Petters, M. D., Carrico, C. M., Hallbauer, E., Massling, A., McMeeking, G. R., Poulain, L., Wu, Z.,
1030 Kreidenweis, S. M., and Stratmann, F.: Towards closing the gap between hygroscopic growth and activation for
1031 secondary organic aerosol: Part 1 – Evidence from measurements, *Atmos. Chem. Phys.*, 9, 3987-3997, 2009.
1032 Wexler, A. S., and Seinfeld, J. H.: 2nd generation inorganic aerosol model, *Atmos. Environ.*, 25, 2731-2748, 1991.
1033 Zhang, Y., Mahowald, N., Scanza, R. A., Journet, E., Desboeufs, K., Albani, S., Kok, J. F., Zhuang, G., Chen, Y.,
1034 Cohen, D. D., Paytan, A., Patey, M. D., Achterberg, E. P., Engelbrecht, J. P., and Fomba, K. W.: Modeling the
1035 global emission, transport and deposition of trace elements associated with mineral dust, *Biogeosciences*, 12, 5771-
1036 5792, 2015.
1037 Zhang, Y. H., Choi, M. Y., and Chan, C. K.: Relating hygroscopic properties of magnesium nitrate to the formation
1038 of contact ion pairs, *J. Phys. Chem. A*, 108, 1712-1718, 2004.
1039 Zieger, P., Vaisanen, O., Corbin, J. C., Partridge, D. G., Bastelberger, S., Mousavi-Fard, M., Rosati, B., Gysel, M.,
1040 Krieger, U. K., Leck, C., Nenes, A., Riipinen, I., Virtanen, A., and Salter, M. E.: Revising the hygroscopicity of
1041 inorganic sea salt particles, *Nature Communications*, 8, 15883, doi: 15810.11038/ncomms15883, 2017.
1042